Thesis for the degree of Doctor of Philosophy

Modelling and Design of High-Power HBV Multipliers

Mattias Ingvarson

CHALMERS

Microwave Electronics Laboratory
Department of Microtechnology and Nanoscience
Chalmers University of Technology
Göteborg, Sweden 2004

Modelling and Design of
High-Power HBV Multipliers
MATTIAS INGVARSON
ISBN 91-7291-531-5

Doktorsavhandlingar vid Chalmers tekniska högskola
Ny serie nr 2213
ISSN 0346-718X

Technical report MC2-11
ISSN 1652-0769
Chalmers University of Technology
Department of Microtechnology and Nanoscience (MC2)
Microwave Electronics Laboratory
SE–412 96 Göteborg, Sweden
Phone: +46–(0)31–772 10 00

Printed in Sweden by
Vasastadens Bokbinderi AB
Göteborg, Sweden, November 2004

Dedicated to the centenary of IFK Göteborg

MODELLING AND DESIGN OF
HIGH-POWER HBV MULTIPLIERS
Mattias Ingvarson
Department of Microtechnology and Nanoscience
Chalmers University of Technology

Abstract

This thesis deals with symmetric varactor frequency multipliers for millimetre and sub-millimetre wave applications. Much of the material presented is general and applicable to any type of (symmetric) varactor, but the focus is on the heterostructure barrier varactor (HBV).
The basic function and principles of HBVs are explained. This includes current transport mechanisms, elastance modulation and the important parasitic series resistance. Various epitaxial material layer structures employed for HBVs are compared, followed by a description of HBV processing techniques and different device geometries. The focus is then directed towards modelling high-power devices and a closely related investigation of thermal limitations and models for HBVs. The thermal properties are important in the subsequent section dealing with the design of HBV layer structures.
HBV frequency multipliers are treated in the last section. Basic multiplier design considerations are discussed, followed by a review of the most common HBV multiplier topologies. Finally, HBV multiplier measurements are described and state-of-the-art results are presented.

Keywords: heterostructure barrier varactor, frequency multiplier, varactor diode, semiconductor, thermal limitations, millimetre and sub-millimetre wave power source.

Preface

This thesis sums up my work as a PhD student at the Microwave Electronics Laboratory at Chalmers 1999-2004. During these years I have had the pleasure to work within the HBV-group under the supervision of Erik Kollberg and Jan Stake. The first two years I was devoted to device fabrication in the old III-V process laboratory. This lab was then closed due to the move to the new MC2 facility, and as a result no fabrication was possible for about one and a half years. I therefore switched focus towards the design and modelling of HBV materials and devices, which is the main topic of the thesis. I have had the opportunity to visit several conferences and to collaborate with colleagues from all over the world, and this has been a great experience for me. Particularly, I have enjoyed the numerous visits to the Rutherford Appleton Laboratory, UK, where we work closely together with the Millimetre Wave Technology Group.

Göteborg, November 15, 2004

Mattias Ingvarson

List of publications

Appended papers

This thesis is based on the following papers:

A. M. Ingvarson, B. Alderman, A. Ø. Olsen, J. Vukusic, and J. Stake, "Thermal constraints for heterostructure barrier varactors",*IEEE Electron Device Letters*, vol. 25, no. 11, pp. 713-715, 2004.

B. M. Ingvarson, A. Ø. Olsen, and J. Stake, "Design and analysis of 500 GHz heterostructure barrier varactor quintuplers", in *Proceedings of the 14th International Symposium on Space Terahertz Technology*, 2003.

C. M. Ingvarson, J. Vukusic, A. Ø. Olsen, T. A. Emadi, and J. Stake, "An electro-thermal HBV model", *manuscript*, 2004.

D. T. Bryllert, A. Ø. Olsen, J. Vukusic, T. A. Emadi, M. Ingvarson, J. Stake, and D. Lippens, "An 11% efficiency 100-GHz InP-based heterostructure barrier varactor quintupler", *submitted to Electronics Letters*, 2004.

E. A. Ø. Olsen, M. Ingvarson, B. Alderman, and J. Stake, "A 100 GHz HBV frequency quintupler using microstrip elements", *IEEE Microwave and Wireless Component Letters*, vol. 14, no. 10, pp. 493-495, 2004.

F. A. Ø. Olsen, M. Ingvarson, and J. Stake, "A low cost fixed tuned F-band HBV frequency tripler", in *IEEE MTT-S International Microwave Symposium Digest*, pp. 899-902, 2003.

G. L. Dillner, W. Strupinski, S. Hollung, C. Mann, J. Stake, M. Beardsley, M. Ingvarson, and E. Kollberg, "Heterostructure barrier varactors on copper substrates for frequency multiplers", in *Proceedings of GHz 2000*, pp. 51-54, 2000.

Other papers

The following papers are not included in the thesis due to an overlap in content or a content going beyond the scope of this thesis:

1. J. Stake, L. Dillner and M. Ingvarson, "Fabrication and characterisation of heterostructure barrier varactor diodes", Chalmers University of Technology, Department of Microwave Technology, Göteborg, Technical Report No. 29 1996, Revised April 2000.

2. J. Stake, C. Mann, L. Dillner, S. Jones, S. Hollung, M. Ingvarson, H. Mohamed, B. Alderman, and E. Kollberg, "Improved diode geometry for planar heterostructure barrier varactors", in *Proceedings of the 10th International Symposium on Space Terahertz Technology*, pp. 485-491, 1999.

3. S. Hollung, J. Stake, L. Dillner, M. Ingvarson, and E. Kollberg,"A distributed heterostructure barrier varactor frequency tripler", *IEEE Microwave and Guided Wave Letters*, vol 48, no. 4, pp. 24-26, 2000.

4. M. Ingvarson, L. Dillner, S. Hollung, E. Kollberg, C. Mann, and J. Stake, "Computer controlled measurements on millimetre and submillimetre wave varactor multipliers", in *Proceedings of GHz 2000*, pp. 297-300, 2000.

5. S. Hollung, J. Stake, L. Dillner, M. Ingvarson, and E. Kollberg, "Novel heterostructure barrier varactor multipliers for millimeter-wave power generation", in *Proceedings of GHz 2000*, pp. 71-74, 2000.

6. L. Dillner, S. Hollung, M. Ingvarson, E. Kollberg, W. Strupinski, C. Mann, and J. Stake, "High efficiency HBV multipliers for millimeter wave generation", in *Proceedings of the 13th International Conference on Microwaves, Radar and Wireless Communications*, pp. 47-54, 2000.

7. W. Strupinski, L. Dillner, J. Sass, K. Kosiel, J. Stake, M. Ingvarson, R. Jakiela "MOVPE strain layers - growth and application", *Journal of Crystal Growth*, vol 221, pp. 20-25, 2000.

8. L. Dillner, M. Ingvarson, E. Kollberg, and J. Stake, "Heterostructure barrier varactor multipliers", in *Proceedings of GaAs 2000*, pp. 197-200, 2000.

9. J. Stake, M. Ingvarson, L. Dillner, and E. Kollberg, "Progress in heterostructure barrier varactor frequency multipliers", in *Proceedings of the 8th International Conference on Terahertz Electronics*, pp. 141-144, 2000.

10. L. Dillner, M. Ingvarson, E. Kollberg, and J. Stake, "High efficiency HBV multipliers for millimetre wave generation", in *Terahertz Sources and Systems*, NATO ASI book series, Kluwer Academic Publishers, 2001.

11. B. Alderman, J. Stake, L. Dillner, D. P. Steenson, M. Ingvarson, E. Kollberg, C. Mann, and J. Chamberlain, "A new pillar geometry for heterostructure barrier varactor diodes", in *Proceedings of the 12th International Symposium on Space Terahertz Technology*, pp. 330-339, 2001.

12. M. Ingvarson, L. Dillner, W. Strupinski, and J. Stake, "Design of material structures for heterostructure barrier varactors", presented at *19th Nordic Semiconductor Meeting*, 2001.

13. A. Ø. Olsen, J. Stake, M. Ingvarson, D. P. Steenson and S. Iezekiel, "A new waveguide integrated microstrip heterostructure barrier varactor (HBV) frequency tripler", in *Proceedings of the 9th International Conference on Terahertz Electronics*, 2001.

14. M. Ingvarson, A. Ø. Olsen, B. Alderman, and J. Stake, " Heterostructure barrier varactor frequency multipliers: materials, devices and circuits", in *Proceedings of GHz 2001*, 2001.

15. A. Ø. Olsen, S. Kazemi, M. Ingvarson, E. Kollberg, and J. Stake, "Planar HBV triplers and quintuplers for millimetre wavelengths", in *Proceedings of the 3rd ESA Workshop on Millimetre Wave Technology and Applications*, pp. 157-162, 2003.

16. A. Laisné, B. Alderman, D. Matheson, B. Ellison, A. Ø. Olsen, M. Ingvarson, and J. Stake "A 500 GHz HBV quintupler", presented at *Terahertz Electronics*, 2003.

17. M. Ingvarson, A. Ø. Olsen, E. Kollberg, and J. Stake, "Design, analysis and modelling of heterostructure barrier varactors for submillimetre wave frequency quintuplers", in *Proceedings of GHz 2003*, 2003.

18. A. Ø. Olsen, M. Ingvarson, E. Kollberg, and J. Stake, "Heterostructure barrier varactor frequency triplers and quintuplers for THz electronics" , in *Proceedings of GHz 2003*, 2003.

19. A. Emadi, J. Vukusic, M. Ingvarson, T. Bryllert, A. Ø. Olsen, E. Kollberg, and J. Stake, "High power HBV multipliers for F- and G- band applications", in *Proceedings of the Joint 29th IRMMW2004 / 12th THz2004*, pp. 319-320, 2004.

Acknowledgement

Three people share the main responsibility for recruiting me to a PhD student position in microwave electronics at Chalmers. These are, in chronological order, Lennart Lundgren, Erik Kollberg and Jan Stake.
I want to thank **Lennart** for his outstanding lectures, for introducing me to the field of microwave electronics, and for being a source of inspiration throughout my years at Chalmers.
Erik employed me as a graduate student 10 years after he invented the device that I have spent the last 5 years exploring. It has been a pleasure to share his great experience and I especially appreciate his support and advice during the last year of research and the writing of this thesis.
I had the intention to finish my master's thesis project, with **Jan** as the supervisor, as soon as possible and then leave Chalmers. Jan, however, had other plans. He used my weakness for English pubs to entice me to continue at Chalmers to work in the HBV factory during the days, and, as it turned out, with child-minding, house-painting, transporting junk etc. during the remaining hours. I am very grateful for his support, inspiration and friendship throughout these years.

None of my research achivements, if any, would have been possible without the help and support from my HBV colleagues at Chalmers. I am most grateful to them all: Lars Dillner, Stein Hollung, Arne Øistein Olsen, Shada Kazemi, Arezoo Emadi, Josip Vukusic and Tomas Bryllert.

I have really appreciated all visits to, and cooperation with, the Rutherford Appleton Laboratory. I have received great hospitality and help, especially from the following, to whom I am deeply obliged: Dave Matheson, Chris Mann, Byron Alderman, John Spencer, Tony Jones, Dave Wilsher, Matthew Beardsley, Brian Landowski and Steve Deane.

Bobby Weikle from the University of Virginia spent a sabbatical year with us at Chalmers, and it was a pleasure to share his great knowledge, ideas and expertise concerning microwave circuits.

I have enjoyed the support and camaraderie from numerous colleagues at Chalmers: Jan Andersson, Stefan Davidsson, Vincent Desmaris, Joakim Eriksson, Christian Fager, Catharina Forssén, Hans Hjelmgren, Lars-Olof Landén, Bente Larsson, Anders Mellberg, Harald Merkel, Niklas Rorsman, Pär Rundqvist, Piotr Starski, Mahdad Sadeghi, Jörgen Stenarson, Klas Yhland, Anders Olausson and Herbert Zirath. Special thanks to Ulf Jordan for help and advice with LaTeX .

Anyone whom I have forgotten to acknowledge properly: Please accept my sincere apologies.

Finally, I would like to thank my friends and family for support.

This work has been supported by the Swedish Foundation for Strategic Research (SSF), the European Space Agency (ESA), and the Swedish Defence Research Agency (FOI).

Contents

Chapter 1

Introduction

Terahertz technology, defined as technology using frequencies from about 100 GHz to several 3 THz, is gradually maturing and already used in many applications [1]. The main applications today are within science, particularly radio astronomy. Applications under development or still at a planning stage are high-speed wireless networks, short-range high-resolution radar systems, medical and biological imaging, high-speed inter-satellite communication, earth environment monitoring, military applications, and surveillance systems, notably security systems. Most such applications crucially depend on the availability of reasonably inexpensive, lightweight and compact sources and detectors. However, as the frequency approaches 1 THz, the output power for both electronic and photonic signal sources drops rapidly. This is commonly referred to as the *THz gap*, cf Figure 1.1. Traditional fundamental signal sources are backward-wave oscillators (BWO) that can generate a few mW at 1.5 THz, and optically pumped lasers for spot frequencies between 0.5 and at least 5 THz with output power in the mW range. However, these sources are heavy, bulky and very expensive. A potential replacement is the quantum cascade laser (QCL) [2] which works very well down to about 3 THz [3], [4] and has the potential to extend the operation down to 1 THz [5]. The major problem is that the present technology requires cryogenic cooling at long wavelengths, which makes QCLs awkward to use. Another approach is photomixing [6], which has shown promising results between 100 GHz and 1 THz, but the output power has only been in the μW range in the best case, apart from a recent demonstration of 20 mW at 100 GHz [7].

The most promising approach to reach the terahertz frequency range with a solid state source is to use a frequency multiplier. Traditionally, this has been accomplished with a reverse-biased Schottky diode [8]. However, the power handling capability of the Schottky device is limited by the device area, which has to be very small at high operating frequencies to allow for manageable impedance levels. From a circuit point of view, higher harmonic multiplication factors ($> \times 3$) become increasingly difficult

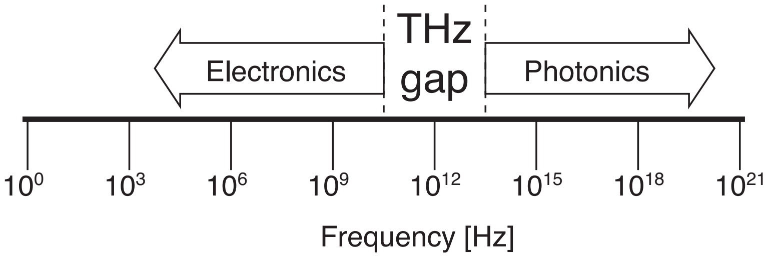

Figure 1.1: The THz gap in the electromagnetic spectrum.

to implement and, therefore, high-order multipliers are usually realised as a chain of several low-order Schottky varactor multipliers [9]. The heterostructure barrier varactor, HBV [10], offers a very competitive alternative to the Schottky varactor for signal generation in the sub-millimetre wavelength region. HBVs utilise material engineering to stack several varactors on top of each other, thus the power handling capacity is increased considerably. Thin barriers of a high band-gap material are positioned between low band-gap regions in a symmetric manner, in order to realise a voltage variable capacitance. This technology has the advantage that for high frequencies and power levels, a large device area can be maintained without a subsequent increase in capacitance. HBVs exhibit a symmetric capacitance-voltage ($C-V$) characteristic and an anti-symmetric current-voltage ($I-V$) characteristic, implying a device that generates only odd harmonics of an applied pump signal. The symmetric layer structure also allows for an unbiased operation. In all, the use of HBVs rather than Schottky varactors greatly simplifies the design of high-order frequency multipliers.

Chapter 2

Varactors

This chapter reviews fundamental varactor theory and presents concepts and definitions that form the basis for the description and modelling of HBV devices and multipliers in the following chapters. The presentation is strongly inspired by the monumental work by Penfield and Rafuse [11]. For further reading, see also [12, 13].

2.1 Basic concepts

A varactor is a device that exhibits a voltage variable, implicitly capacitive, reactance. A varactor is typically a semiconductor diode, which can be used for harmonic generation, frequency conversion, parametric amplification, detection and voltage-variable tuning [11]. During operation, currents of many frequencies can be present in the varactor. Some of these currents are useful inputs or outputs, while some are *idlers*. Idlers can, however, be necessary for optimum operation of the device.

2.1.1 Manley-Rowe formulae

The Manley-Rowe formulae [14] relate power flowing into and out of nonlinear reactances. The relations apply to ideal, i. e. loss-less, varactors where current and voltage are assumed to exist at frequencies $mf_1 + nf_2$, where m and n are integers. The formulae are

$$\sum_{m=1}^{\infty} \sum_{n=-\infty}^{\infty} \frac{mP_{\mathrm{m,n}}}{nf_1 + mf_2} = 0 \tag{2.1}$$

$$\sum_{m=-\infty}^{\infty} \sum_{n=1}^{\infty} \frac{nP_{\mathrm{m,n}}}{nf_1 + mf_2} = 0. \tag{2.2}$$

$P_{\mathrm{m,n}}$ is the average power flowing into the varactor at the frequency $mf_1 + nf_2$. For a frequency multiplier all frequencies are harmonics of only one frequency, f_1, thus $m = 0$, and the Manley-Rowe relations become $P_1 + P_{\mathrm{n}} = 0$. That is, if the circuit is designed so that only real power can flow at the input frequency f_1 and at the output frequency nf_1, the Manley-Rowe formulae predict a conversion efficiency of 100%. It should be noted, however, that the Manley-Rowe formulae do not take any DC power into account. This means that the power at any output frequency nf_1 cannot be increased by supplying DC power.

2.2 Pure varactor model

The equivalent circuit of a pure varactor, i. e. a varactor with no conduction current, has two elements, see Figure 2.1. This simple model consists of a constant series resistance, R_{s}, and a nonlinear differential elastance, $S(V) = dV/dQ = 1/C(V)$, where V is the voltage applied across the diode. (Since the equivalent varactor model contains a capacitance in series with a resistance, it is common to talk about elastance rather than capacitance). The model can be used to describe the basic behaviour of a varactor, and is valid when the displacement current is much larger than the conduction current across the diode junction. An important and extensively used figure-

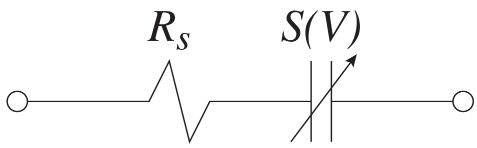

Figure 2.1: Equivalent circuit for a pure varactor.

of-merit for varactors is the dynamic cut-off frequency, f_{c}, which is defined as

$$f_{\mathrm{c}} = \frac{S_{\max} - S_{\min}}{2\pi R_{\mathrm{s}}} \tag{2.3}$$

where $S_{\max}$ and $S_{\min}$ are the maximum and minimum elastances, respectively, and R_{s} is the series resistance. Thus, a good varactor should have a large elastance swing, $S_{\max}$-$S_{\min}$, and a low series resistance. A state-of-the-art varactor has a cut-off frequency of several THz.

2.3 Practical varactors

One distinguishes between varactors with asymmetric and symmetric $C-V$ characteristics. Reverse-biased Schottky and p$^+$n diodes are the most common asymmetric varactors, whereas HBVs and back-to-back Schottky diodes are examples of symmetric varactors. Figure 2.2 shows the elastance versus voltage characteristics for conventional and symmetric varactors, respectively.

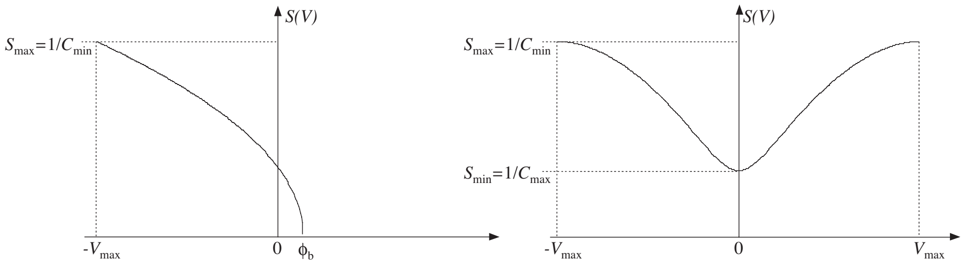

Figure 2.2: Elastance versus voltage for (left) a conventional (asymmetric) varactor and (right) a symmetric varactor.

2.4 Pumping

The process where a large current at an angular pump frequency $\omega_\mathrm{p} = 2\pi f_\mathrm{p}$ is passed through the varactor is called *pumping*. This is the normal mode of operation for a varactor in a frequency multiplier. During a pump cycle, the varactor behaves as a time-varying elastance, $S(t)$, and power is dissipated in the series resistance. The voltage across the pure varactor in Figure 2.1 is then

$$v(t) = R_\mathrm{s} i(t) + \int S(t) i(t) dt. \tag{2.4}$$

The boundary conditions to (2.4) are equations describing how the varactor is terminated at the harmonics involved. These equations, however, are more conveniently described in the frequency domain. In a frequency multiplier only frequencies that are multiples of the pump frequency, i. e. $k \cdot \omega_\mathrm{p}, k \in \mathbb{N}$, are present. The voltage, current and differential elastance can therefore be written as Fourier series:

$$v(t) = \sum_{k=-\infty}^{\infty} V_\mathrm{k} e^{jk\omega_\mathrm{p} t}, \tag{2.5}$$

$$i(t) = \sum_{k=-\infty}^{\infty} I_\mathrm{k} e^{jk\omega_\mathrm{p} t} \tag{2.6}$$

and

$$S(t) = \sum_{k=-\infty}^{\infty} S_\mathrm{k} e^{jk\omega_\mathrm{p} t}, \tag{2.7}$$

where $V_{-\mathrm{k}} = V_\mathrm{k}^*$, $I_{-\mathrm{k}} = I_\mathrm{k}^*$ and $S_{-\mathrm{k}} = S_\mathrm{k}^*$ as $v(t)$, $i(t)$ and $S(t)$ are real quantities. Thus, the Fourier coefficients of V can be written

$$V_\mathrm{k} = R_\mathrm{s} I_\mathrm{k} + \frac{1}{jk\omega_\mathrm{p}} \sum_{l=-\infty}^{\infty} I_\mathrm{l} S_{\mathrm{k}-\mathrm{l}}. \tag{2.8}$$

2.5 Symmetric varactor frequency multipliers

This section reviews some basic concepts applicable to symmetric varactor frequency multipliers, notably HBV multipliers.

2.5.1 Conversion efficiency

The conversion efficiency η is defined as the power delivered to the load at the desired output frequency, $n \times f_{\mathrm{p}}$, divided by the available input power at f_{p}. The maximum conversion efficiency for varactor multipliers is related to the ratio of the pump frequency f_{p} and the dynamic cut-off frequency f_{c} [11,15]. The following empirical expression is useful for initial estimations [16],[Paper B]:

$$\eta = \frac{100}{1+\alpha\left(\dfrac{n \cdot f_{\mathrm{p}}}{3 \cdot f_{\mathrm{c}}}\right)^{\beta}}, \tag{2.9}$$

where α and β can be extracted from large-signal simulations for various (HBV) devices and circuit conditions. For $f_{\mathrm{p}}/f_{\mathrm{c}} < 0.2$, we typically find $\alpha = 200$ and $\beta = 1.5$ for HBV triplers [16].

2.5.2 Elastance models

It is of interest to investigate how the shape of elastance-voltage ($S-V$) characteristics influence the conversion efficiency of varactor frequency multipliers. In order to facilitate such studies it is advantageous to use simple, generally defined $S-V$ models. One such model is the cubic varactor model for the voltage V as a function of the stored charge Q in the varactor [17], which is based on the third-order voltage-charge model suggested by Tang *et al.* [18]. The cubic model can be extended to a fifth degree polynomial model to allow for varying the shape of the $S-V$ characteristics:

$$V(Q) = S_{\mathrm{min}}Q + (S_{\mathrm{max}} - S_{\mathrm{min}})\left(\xi\frac{Q^3}{Q_{\mathrm{max}}^2} + \chi\frac{Q^5}{Q_{\mathrm{max}}^4}\right) \tag{2.10}$$

where

$$Q_{\mathrm{max}} = \frac{V_{\mathrm{max}}}{S_{\mathrm{min}} + (S_{\mathrm{max}} - S_{\mathrm{min}})(\xi+\chi)}. \tag{2.11}$$

Q_{max} is the charge stored in the varactor at the maximum voltage, V_{max}, during a pump cycle, and ξ and χ are fitting coefficients. For (2.10) to describe an HBV correctly, the differential elastance must increase monotonically with increasing charge. This constraint gives two extreme cases for fixed values of S_{min} and S_{max}, denoted *flat* $S-V$ and *sharp* $S-V$, respectively. ξ and χ for the three elastance models mentioned are summarised in Table 2.1. Figure 2.3 displays elastance waveforms obtained from (2.10) with the coefficients taken from Table 2.1. The sharp $S-V$ model gives the highest conversion efficiency in varactor multipliers [15].

Table 2.1: Constants for the three $S-V$ models for (2.10).

	ξ	χ
Flat	0	1/5
Cubic	1/3	0
Sharp	2/3	-1/5

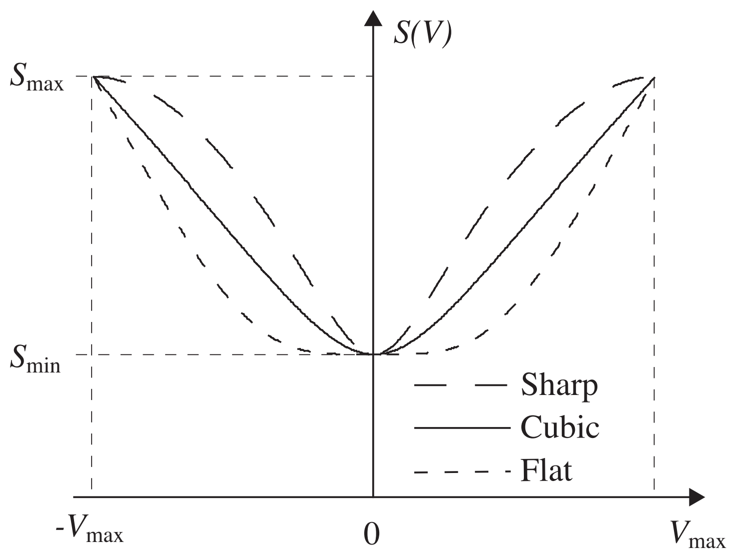

Figure 2.3: S-V characteristics for the three models generated from (2.10).

2.5.3 Losses caused by conduction current

Any practical varactor has a non-zero conduction current, which causes losses and thereby degrades the multiplier performance. This conduction current can be modelled as a voltage dependent conductance in parallel with the nonlinear, differential elastance of the pure varactor model, see Figure 2.4. In this extended model, the differential elastance $S(V)$ has been

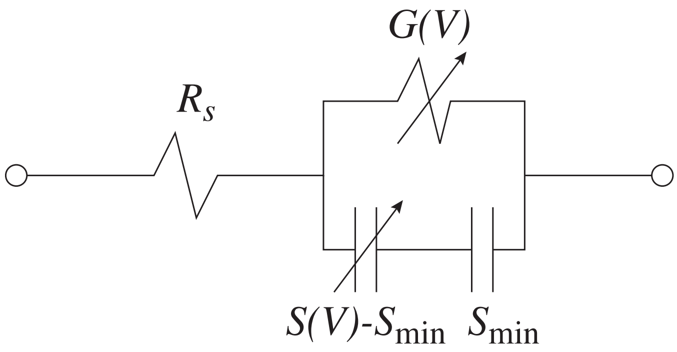

Figure 2.4: Extended varactor model.

split up in two parts, where S_{min} is the minimum elastance which appears at zero bias. The conductance increases with increasing bias, cf Figure 3.6, implying that the maximum conductance occurs at the maximum bias,

$$G_{\mathrm{max}} = \frac{I_{\mathrm{max}}}{V_{\mathrm{max}}}. \tag{2.12}$$

If the conductance is assumed to be constantly equal to the maximum value, (2.12), it is possible to estimate an upper limit of the losses caused by the conduction current. As a rule of thumb, if $G_{\mathrm{max}} \lesssim \omega_{\mathrm{p}} \cdot C_{\mathrm{min}} \cdot 0.01$, the extra loss introduced by G_{max} is less than approximately 0.3 dB [19].

Chapter 3

Heterostructure barrier varactors

The heterostructure barrier varactor (HBV) was invented in 1989 by Erik Kollberg, [10], as a spin-off from the research on resonant tunnelling devices. An HBV is a symmetric device composed of a high band-gap semiconductor (*barrier*) that is surrounded by low band-gap semiconductors (*modulation layers*), see Figure 3.1, for typical dimensions see Table 3.2. The first HBVs had only one barrier and were therefore referred to as *single-barrier varactors*, SBVs. Another obsolete term that is sometimes encountered in the literature is *quantum-barrier varactors*, QBVs. Practical HBVs typically have 1-6 barriers. The layer structure is grown by molecular beam epitaxy (MBE) or metal-organic vapour phase epitaxy (MOVPE). Thanks to the rapid progress in these epitaxial growth techniques during the last decade, it is now possible to grow HBV materials of high quality [20–23]. So far, HBVs have exclusively been realised in III-V material systems, although $Si/SiO_2/Si$ devices conceptually similar to III-V HBVs have been investigated to some extent [24].

3.1 Principle of operation

Consider a one-barrier HBV, i. e. one barrier symmetrically sandwiched between two modulation layers. The barrier acts as a potential barrier for the electrons, and thus prevents electron transport through the structure. When an external bias V is applied across the device, electrons are accumulated at one side of the barrier and depleted at the other side, see Figure 3.2. The device thus has a voltage-dependent depletion region in the modulation layer, implying a voltage-dependent $C-V$ characteristic. The symmetry of the layer structure gives a symmetric $C-V$ characteristic, i. e. an HBV is a symmetric varactor. The main current transport mechanisms in an HBV are thermionic emission of electrons over the barrier and electron tunnelling

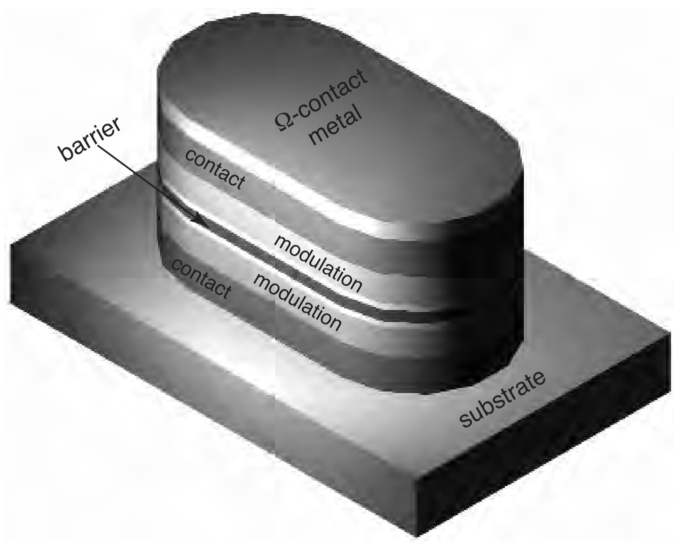

Figure 3.1: CAD view of a one-barrier HBV mesa. For typical dimensions, see Table 3.2.

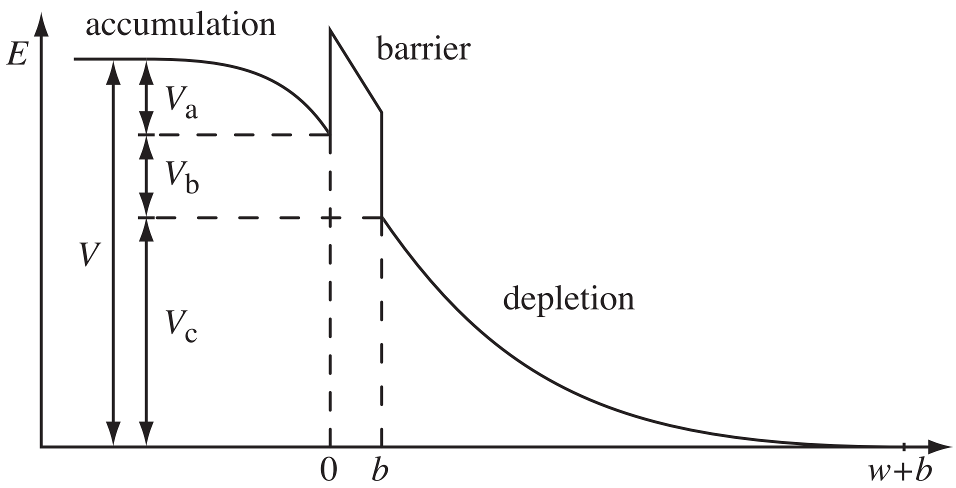

Figure 3.2: Conduction band of a one-barrier HBV. w is the width of the depletion region.

through the barrier. The device temperature, applied bias and the effective height and thickness of the barrier determines the dominating mechanism. In order to maximise the power handling capacity, the HBV material should have several barriers stacked in series, and a relatively low doping concentration in the modulation layers to increase the breakdown voltage. However, if too many barriers are used, the device temperature increases, and this degrades the diode's varactor properties. For a given material structure it is possible to estimate the maximum number of barriers that can be used without degrading the HBV [Paper A]. If the modulation layers are made shorter and doped more heavily, the losses and the effect of current saturation for high frequency applications are reduced [25, 26].

3.1.1 Equivalent circuit models

The most simple equivalent circuit model for HBVs is the the pure varactor model presented in Figure 2.1, which can be used to describe the basic properties. A more accurate model, useful for numerical analysis of HBVs, is the nonlinear, quasi-static model displayed in Figure 3.3. The current source models the leakage current through the device. A more extensive

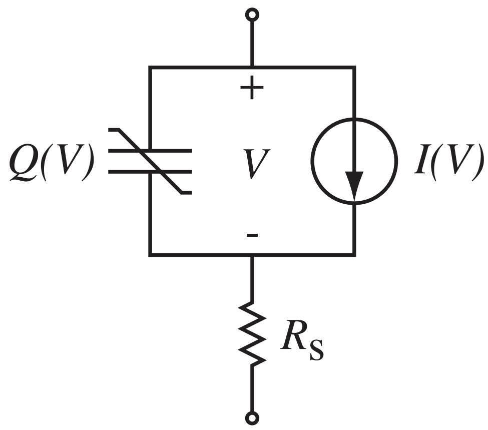

Figure 3.3: Quasi-static equivalent circuit model of an HBV.

model is displayed in Figure 3.4. This model can be extracted from measured reflection coefficients [27]. Here, the dependence on temperature and frequency is included, as well as parasitic elements. The series resistance is frequency-dependent due to the skin effect, and voltage-dependent due to the extension of the depletion region. The series inductance L_p models the connection to the diode, i. e. bonding wire or air-bridge, and the shunt capacitance C_p represents parasitic capacitances due to packaging.

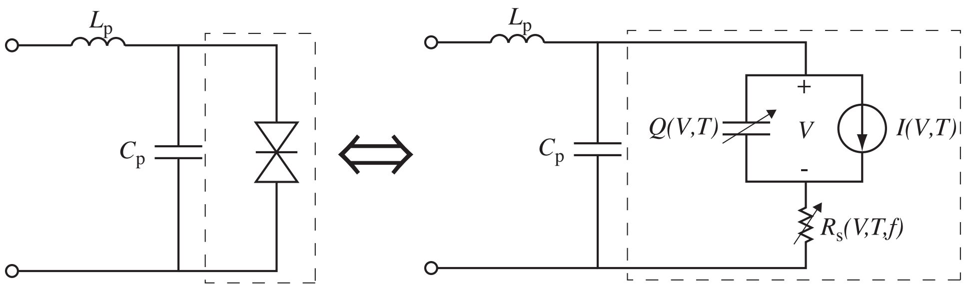

Figure 3.4: Extended quasi-static equivalent circuit model of an HBV.

3.1.2 Capacitance-voltage characteristics

The symmetric $C-V$ characteristic of a typical HBV is shown in Figure 3.5. The appearance of the HBV capacitance can be understood by considering

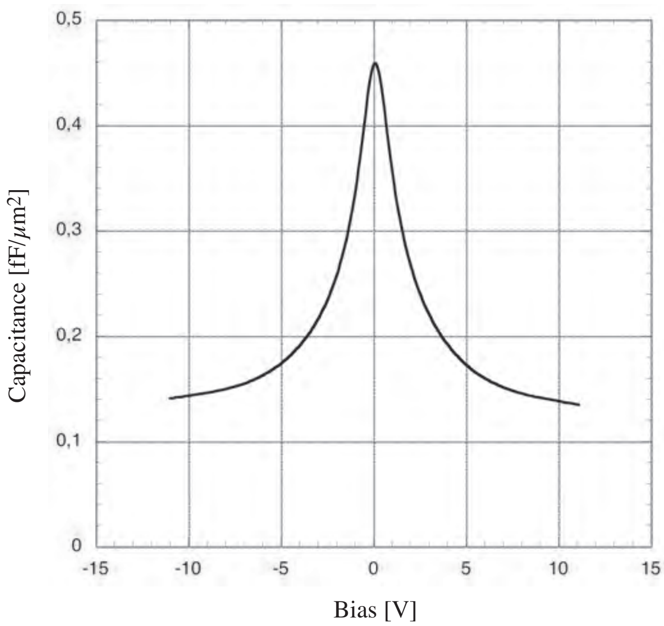

Figure 3.5: Measured capacitance per unit area versus applied voltage for a typical HBV diode. The material is a four-barrier InGaAs/InAlAs heterostructure on an InP substrate, CTH-ITME-1820.

the parallel plate capacitor model. The plate separation is equivalent to the sum of the barrier thickness, b, the spacer layer thickness, s, see Table 3.2, and the length of the depletion region in the modulation layer, w. Due to the symmetric layer structure of HBVs, the differential elastance is an even function of the applied voltage,

$$S(V) = \frac{1}{C(V)} = \frac{N}{A}\left(\frac{b}{\varepsilon_{\mathrm{b}}} + \frac{s}{\varepsilon_{\mathrm{d}}} + \frac{w(V)}{\varepsilon_{\mathrm{d}}}\right), \tag{3.1}$$

where N is the number of barriers, A is the device area, and ε_b and ε_d are the dielectric constants of the barrier and modulation layer materials, respectively. Equation (3.1) is not accurate close to zero bias. w can be calculated from

$$w = \sqrt{\frac{2\varepsilon_\mathrm{d}\,|V_\mathrm{d}|}{qN_\mathrm{d}}}, \tag{3.2}$$

where V_d is the voltage across the depleted region of each modulation layer, q is the elementary charge and N_d is the doping concentration in the modulation layers. The minimum elastance S_min occurs at zero bias, i. e. w=0. However, due to electron screening effects, a more accurate expression for S_min must include the extrinsic Debye length L_D,

$$L_\mathrm{D} = \sqrt{\frac{\varepsilon_\mathrm{d} kT}{q^2 N_\mathrm{d}}}, \tag{3.3}$$

where k is the Boltzmann constant and T is the device temperature. Thus

$$S_\mathrm{min} = \frac{N}{A}\left(\frac{b}{\varepsilon_\mathrm{b}} + \frac{2s}{\varepsilon_\mathrm{d}} + \frac{2L_\mathrm{D}}{\varepsilon_\mathrm{d}}\right). \tag{3.4}$$

The maximum elastance S_max during a pump cycle is determined by the drive level of the HBV, defined as

$$drive = \frac{\max(Q(t))}{Q_\mathrm{max}} \tag{3.5}$$

where Q_max is the charge at the turn-on voltage, $V_\mathrm{j,max}$ [16]. Optimum performance is achieved with a maximum elastance swing, low conduction current and *drive*=1. Under these conditions, the maximum elastance is limited by

$$S_\mathrm{max} = \frac{N}{A}\left(\frac{b}{\varepsilon_\mathrm{b}} + \frac{s}{\varepsilon_\mathrm{d}} + \frac{w_\mathrm{max}}{\varepsilon_\mathrm{d}}\right) \tag{3.6}$$

where w_max is the maximum extension of the depletion region, determined by one of the following conditions:

1. Modulation layer punch-through, i. e. the modulation layer is fully depleted so that w_max=l where l is the thickness of the modulation layer;

2. Large electron conduction current across the barrier due to thermionic emission at high electric fields;

3. Large electron conduction current originating from impact ionisation at high electric fields;

4. Current saturation, i. e. the saturated electron velocity determines the maximum length an electron can travel during a pump cycle.

All four of the above conditions are valid for GaAs-based HBVs, whereas condition 2 is usually not applicable for InP-based devices due to the much higher effective barrier height. For condition 2, the conduction current depends on the effective barrier height and the electric field in the barrier [28]. For condition 3, w_{max} can be calculated as

$$w_{\mathrm{max}} = \frac{\varepsilon_{\mathrm{d}} E_{\mathrm{d,max}}}{q N_{\mathrm{d}}} \tag{3.7}$$

where $E_{\mathrm{d,max}}$ is the maximum electric field in the modulation layer at the voltage where breakdown occurs. For condition 4, w_{max} can be estimated as

$$w_{\mathrm{max}} \approx \frac{v_{\mathrm{max}}}{8 f_{\mathrm{p}}} \tag{3.8}$$

where v_{max} is the saturated electron velocity [25].

The Chalmers HBV model, (3.9), is a quasi-empirical expression for the voltage V across an HBV expressed as a function of the charge Q stored in the device [29]:

$$\begin{aligned} V(Q) = N\Bigg(& \frac{bQ}{\varepsilon_{\mathrm{b}} A} + 2\frac{sQ}{\varepsilon_{\mathrm{d}} A} \\ & + \mathrm{sign}(Q)\left(\frac{Q^2}{2qN_{\mathrm{d}}\varepsilon_{\mathrm{d}}A^2} + \frac{4kT}{q}\left(1 - \exp\left[-\frac{|Q|}{2L_{\mathrm{D}}AqN_{\mathrm{d}}}\right]\right)\right)\Bigg). \end{aligned} \tag{3.9}$$

Equation (3.9) is useful for numerical analysis of HBVs, e. g. harmonic balance.

3.1.3 Current-voltage characteristics

The $I - V$ characteristic of an HBV is anti-symmetric. Its appearance is mainly caused by thermionic emission of electrons over the barrier and/or tunnelling of electrons through the barrier. The device temperature, applied bias and the height and thickness of the barrier determine which current transport mechanism is dominant in each situation. An $I - V$ characteristic of a typical HBV is shown in Figure 3.6. Given a general barrier structure and adjacent modulation layers, it is possible to calculate the $I - V$ characteristic with numerical techniques [30–32]. The conduction current can be calculated by solving the Poisson equation and the Schrödinger equation [33]. Attempts to solve the Poisson and Schrödinger equations self-consistently for an applied AC bias have been carried out [34], but this approach is not yet feasible for design work. Instead, empirical, quasi-static $I - V$ models have to be used to predict the RF performance of HBVs. For GaAs/AlGaAs on GaAs HBVs, where thermionic field emission is the dominant current transport mechanism, the following model can be used to calculate the conduction

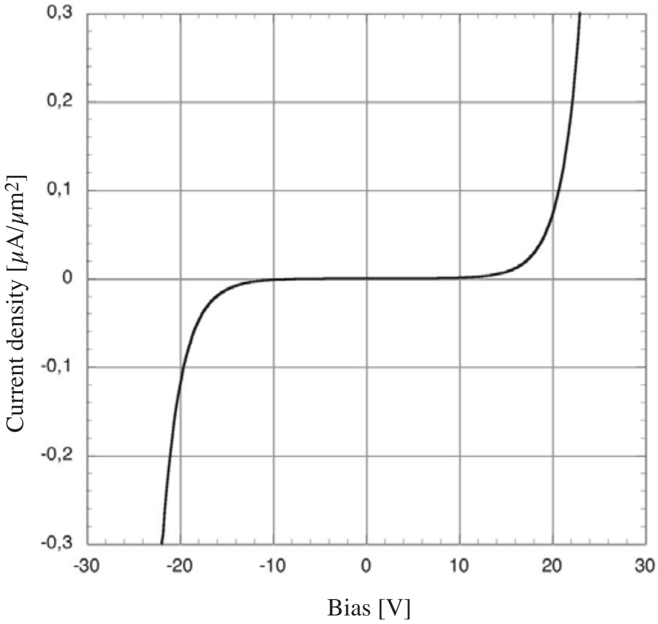

Figure 3.6: Measured current density versus voltage for a typical HBV diode. The material is a four-barrier InGaAs/InAlAs heterostructure on an InP substrate, CTH-ITME-1820.

current density:

$$J_{\mathrm{cond,GaAs}} = aT^2 \sinh\left(\frac{E_\mathrm{b}}{E_0}\right) \exp\left(-\frac{\phi_\mathrm{b}}{kT}\right) \tag{3.10}$$

where E_b is the electric field in the barrier and a, E_0 and ϕ_b are constants [29]. The constants can be extracted from Arrhenius plots of the measured current density at different temperatures. E_b can be estimated from the Poisson equation as

$$E_\mathrm{b} = \frac{N_\mathrm{d} q \varepsilon_\mathrm{d} b}{\varepsilon_\mathrm{b}^2} \left(\sqrt{1 + \frac{2V\varepsilon_\mathrm{b}^2}{N_\mathrm{d} q \varepsilon_\mathrm{d} b^2 N}} - 1 \right), \tag{3.11}$$

or explicitly from the charge as $E_\mathrm{b} = Q/(\varepsilon_\mathrm{b} A)$. For InGaAs/AlInAs on InP HBVs, the conduction current can be described by

$$J_{\mathrm{cond,InP}} = a \cdot \exp\left(\frac{T}{T_0}\right) \sinh\left(\frac{V}{V_0}\right) \tag{3.12}$$

where a, T_0 and V_0 are constants [35]. Figure 3.7 shows a comparison between the conduction current of a 4-barrier GaAs-based HBV (UVA-NRL-1174) and a 3-barrier InP-based HBV (CTH-ITME-1596). The curves where

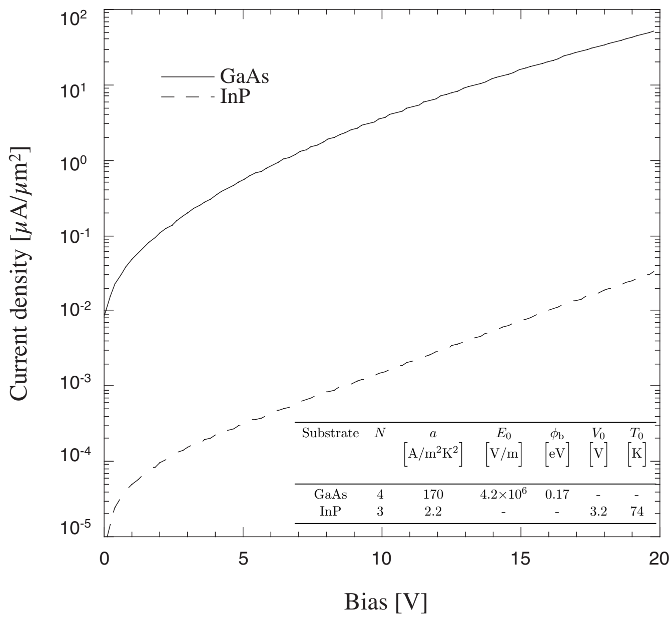

Figure 3.7: Conduction current for a 4-barrier GaAs-based HBV and a 3-barrier InP-based HBV.

calculated from (3.10) and (3.12), respectively, assuming room temperature operation. The displacement current can be calculated using harmonic balance, from

$$i(t) = \frac{\partial Q}{\partial t}. \tag{3.13}$$

3.1.4 Series resistance

The series resistance R_s associated with a diode is a quantity which summarises the resistive losses that characterise the various layers forming the device. For varactors, R_s is one of the most important limiting parameters. According to (2.3), R_s must be minimised in order to maximise the dynamic cut-off frequency. This is especially important for higher frequencies, since the available pump power decreases rapidly with increasing frequency. The main contributors to the series resistance are the ohmic contact resistance, the resistance in the modulation and contact/buffer layers and the spreading resistance. The ohmic contact resistance R_c is strongly affected by the fabrication process. In order to minimise R_c, it is important to use an optimum metallic scheme and optimum annealing conditions [36]. The resistance in the modulation layers can be reduced by using as thin layers as possible with respect to the capacitance modulation, a high-mobility material, and a relatively high doping concentration. However, a too high doping concentration and too thin modulation layers result in a low breakdown voltage and a low maximum elastance. Therefore, there is a trade-off between high power handling capacity and low losses. The spreading resistance is caused by the material near the anode and, at high frequencies, the skin effect has to be included [37], which means that the diode geometry becomes important. Given the voltage-charge relationship in (3.9), the series resistance can be expressed as [16]

$$R(Q) = R_\mathrm{s} - \frac{\rho_\mathrm{d} N}{A}\left(\frac{|Q|}{qN_\mathrm{d}A} + 2L_\mathrm{D}\left(\exp\left[-\frac{|Q|}{2L_\mathrm{D}AqN_\mathrm{d}}\right] - 1\right)\right) \tag{3.14}$$

where R_s is the zero-bias intrinsic series resistance and ρ_d is the resistivity of the modulation layer,

$$\rho_\mathrm{d} = \frac{1}{qN_\mathrm{d}\mu_\mathrm{e}(N_\mathrm{d}, T)}. \tag{3.15}$$

The electron low-field mobility $\mu_\mathrm{e}(N_\mathrm{d}, T)$ can be calculated from the following empirical model [38]

$$\mu_\mathrm{e}(N_\mathrm{d}, T) = \mu_\mathrm{min} + \frac{\mu_\mathrm{max}(T_0)(T_0/T)^{\theta_1} - \mu_\mathrm{min}}{1 + \left(\dfrac{N_\mathrm{d}}{N_\mathrm{ref}(T_0)(T/T_0)^{\theta_2}}\right)^{\lambda}}. \tag{3.16}$$

Here, μ_min, μ_max, N_ref, λ, θ_1 and θ_2 are fitting parameters available for most common III-V materials, and $T_0 = 300\mathrm{K}$. It is very difficult to measure the series resistance. For varactors that can be probed, R_s can be extracted from reflection coefficient measurements with a network analyser [27]. However, a sensitivity analysis [36] shows that the accuracy from an S-parameter analysis can never be better than

$$\frac{\Delta R_\mathrm{s}}{R_\mathrm{s}} = \frac{(R_\mathrm{s} + Z_0)^2}{2R_\mathrm{s}Z_0}\Delta\Gamma \tag{3.17}$$

where Z_0 is the characteristic (system-) impedance and $\Delta\Gamma$ is the estimated measurement error in the reflection coefficient Γ. Equation (3.17) is valid for Q-values below the optimum Q-value for capacitance estimations, which is approximately

$$\frac{1}{\omega C} = Z_0. \tag{3.18}$$

Another way to estimate the series resistance is to combine data from contact resistance measurements with resistivity data for the semiconductors used.

At terahertz frequencies, other effects become important. The performance can be degraded by plasma resonances in the epilayers and current saturation. The latter effect can be modelled as an effective series resistance, which increases rapidly with increasing pump power [25].

3.1.5 Electro-thermal HBV modelling

In order to properly analyse and design HBV devices and circuits, especially for high-power applications, it is necessary to combine electrical and thermal simulations. We have demonstrated the first such model, [Paper C], which automatically updates the temperature and temperature-dependent parameters as the series resistance and the conduction current. The model is implemented in ADS from Agilent and can accurately reproduce measured results.

3.1.6 Physical modelling of HBVs

Physical modelling can give important information about, and insight into, the behaviour of semiconductor devices under various operating conditions. Jones *et al.* have developed a time-dependent numerical drift/diffusion HBV model, integrated with a large-signal harmonic balance circuit simulator [39–41]. In order to accurately model carrier transport at high frequencies, the effect of hot electron transport should be included. For Schottky diodes, this has been accomplished by means of Monte-Carlo simulations [42] and by including energy balance equations [30]. These techniques can also be employed, but are still unexplored, for HBVs.

3.2 Material systems

So far, all working HBVs have been fabricated from a combination of III-V semiconductors. Important data for some materials of interest for HBVs is presented in Table 3.1. The layer structures are grown with epitaxial growth techniques, mainly molecular beam epitaxy, MBE, and metal-organic vapour phase epitaxy, MOVPE. The properties of HBV devices depend strongly on the quality of the layer structure material. Thanks to the extensive progress in these epitaxial growth techniques during the last decade, it is now possible to realise relatively complicated HBV materials with sufficient accuracy and quality. However, new material combinations are continuously being investigated, in order to find ways to minimise the series resistance and the leakage current, to maximise the breakdown voltage, to improve the high frequency properties, etc. In principle, any symmetrical material combination with a band-gap discontinuity can be chosen. Yet, an important constraint is that the lattice mismatch must not be too large in order to avoid stress in the structure. If the layer thickness of a certain material reaches the material's critical thickness, the layer relaxes to its natural lattice constant, causing dislocations in the material. Stress also causes piezoelectric fields, which may alter the energy band structure, and thus the electrical characteristics of the device. Table 3.2 shows a generic layer structure for InP and GaAs based HBVs. A review of commonly used, and some more exotic, HBV

Table 3.1: Bulk properties of some materials at room temperatures.

Material	E_g [eV]	μ [cm^2/Vs]	v_{max} [cm/s]	ε_r	κ [W/cmK]
Si	1.12	1450	8×10^6	11.9	1.5
Ge	0.66	3900	6×10^6	16.2	0.6
6H-SiC	3.03	900	2×10^7	9.66	5
Diamond	5.5	2200	2.7×10^7	5.7	10-20
SiO_2	9	-	-	3.9	0.014
AlP	2.45	60	-	9.80	0.9
AlAs	2.15	290	-	10.06	-
AlSb	1.62	200	-	12.04	0.3
AlN	6.2	135	1.7×10^7	8.5	2
2H-GaN	3.44	1000	3×10^7	8.9	1.5
GaP	2.27	160	-	11.1	1
GaAs	1.42	9200	1.8×10^7	12.85	0.46
GaSb	0.75	3750	-	15.69	0.4
InP	1.34	5900	2.5×10^7	12.56	0.7
InAs	0.35	33000	3.6×10^7	15.15	0.3
InSb	0.18	77000	5×10^7	16.80	-

materials is given in the following sections.

Table 3.2: Generic layer structure for a typical one-barrier HBV. For an N-barrier device, the layer sequence 2-7 is repeated N times. y∈[0.4,0.7].

	Layer	Substrate InP	Substrate GaAs	Thickness [Å]	Doping [cm^{-3}]
9	Contact	$In_xGa_{1-x}As$ x:1⟶0.53	$In_xGa_{1-x}As$ x:1⟶0	5000	n^{++}
8	Modulation	$In_{0.53}Ga_{0.47}As$	GaAs	3000	$\gtrsim 10^{17}$
7	Spacer	$In_{0.53}Ga_{0.47}As$	GaAs	50	Undoped
6	Barrier	$In_{0.52}Al_{0.48}As$	$Al_yGa_{1-y}As$	50/30	Undoped
5	Barrier	AlAs	AlAs	30	Undoped
4	Barrier	$In_{0.52}Al_{0.48}As$	$Al_yGa_{1-y}As$	50/30	Undoped
3	Spacer	$In_{0.53}Ga_{0.47}As$	GaAs	50	Undoped
2	Modulation	$In_{0.53}Ga_{0.47}As$	GaAs	3000	$\gtrsim 10^{17}$
1	Contact	$In_{0.53}Ga_{0.47}As$	GaAs	5000	n^{++}
0	Substrate	InP	GaAs		n^{++} or S.I.

3.2.1 GaAs/AlGaAs on GaAs

GaAs is a well characterised and extensively used semiconductor, which is mechanically stable and relatively easy to process. Therefore, the first HBVs where fabricated using GaAs-based layer structures [10, 43]. This system is lattice matched, which means that stress-free layers can be grown. The main disadvantage is the low height of the GaAs/AlGaAs/GaAs potential barrier. Due to the low barrier height, the leakage current is large, which degrades the frequency multiplier performance. By incorporating a thin layer of AlAs in the AlGaAs barrier, it is possible to double the effective barrier height [44]. The barrier height can be increased further by using thin layers of a low band-gap semiconductor on each side of the barrier, e.g. In_xGaAs [45, 46].

3.2.2 InGaAs/InAlAs on InP

State-of-the-art HBVs are fabricated in the $In_xGa_{1-x}As/In_yAl_{1-y}As$ on InP system. Almost exclusively, x=0.53 and y=0.52, as these compositions are lattice matched to InP. Electron velocities are higher in InGaAs than in GaAs and the barrier is higher, which means lower leakage currents and, thus, improved frequency multiplier performance. HBVs with very good low leakage currents have been fabricated in this material system [33,47]. A thin, pseudomorphic layer of AlAs in the middle of the barrier increases the barrier height even further. Because of the high potential barrier, HBVs fabricated from this system are less sensitive to self-heating, and excellent frequency tripler performance has been reported [21, 35, 48]. The main drawbacks are that InP substrates are more expensive and fragile than GaAs substrates, and it is more difficult to grow thick epilayers. However, thick, high quality HBV materials have been grown by MOVPE [49–51]. The $C_{\max}/C_{\min}$ ratio, which affects the cut-off frequency, can be improved with a planar doping and a quantum well adjacent to the barrier [52], although the escaping and trapping mechanisms of such quantum wells at high frequencies have not yet been fully investigated. A major drawback, especially for high-power applications, is the poor thermal conductivity κ of $In_{0.53}Ga_{0.47}As$, of a tenth of that of GaAs, see Table 3.1.

3.2.3 InAs/AlSb on InAs

AlSb and InAs are slightly mismatched, but layers of a few hundred Å can be grown without dislocations. Advantages with this material system are the high intrinsic mobility and the high electron drift velocity in InAs, combined with a large band edge offset in the conduction band. However, AlSb/InAs is a type II heterojunction, which implies that the valence band edge offset is negative. Therefore, there is no hole barrier to block the hole current, and a thin layer of AlAs must be inserted in the barrier. AlSb oxidises quickly and therefore needs protection. This, combined with a low breakdown voltage and complicated processing techniques, makes InAs/AlSb on InAs less usefull for HBV fabrication. Attempts to demonstrate high conversion efficiencies have been made [53], but hitherto no successful HBVs have been produced in this material system.

3.2.4 Metamorphic InGaAs/InAlAs on GaAs

GaAs substrates are preferred because of the lower cost, larger available wafers and better mechanical properties compared to InP. It is possible to grow lattice mismatched, dislocation free InGaAs/InAlAs epilayers on GaAs substrates for various applications [54, 55]. This can be done by growing a buffer layer in InGaAs or InAlAs, where the material composition is gradually changed, from GaAs to a material with the desired lattice constant. With this technique, material systems with an arbitrary In content in the modulation layers can be grown. The quality of graded buffer layers grown by MBE is good, but the technology is relatively new. A disadvantage however, is the high thermal resistance of the InGaAs or InAlAs buffer layer. So far, no HBVs have been successfully fabricated using this kind of material.

3.2.5 Wide band-gap materials: AlGaN/GaN

Wide band-gap systems such as AlGaN on GaN offer new possibilities for HBVs in terms of very low leakage currents due to a high effective barrier height, and a high power capacity due to the excellent thermal conductivity and the wide band-gap. Drawbacks are low electron mobility, high cost, and piezoelectric fields which alter the electric properties of HBVs [56].

3.2.6 Ferroelectric varactors

Ferroelectric materials are characterised by an electric field and temperature dependent dielectric constant. Thin films of $Ba_xSr_{1-x}TiO_3$ (BSTO) or $SrTiO_3$ (STO) can be used to fabricate ferroelectric varactors with properties similar to those of HBVs, i. e. symmetric $C - V$ characteristics [57, 58].

3.2.7 Si/SiO_2 on Si

A symmetric structure similar to III-V HBV heterostructures can be fabricated by bonding two thin silicon wafers with silicondioxide on the bonding surfaces [24]. SiO_2 is an excellent barrier material, which blocks current very efficiently, but the main drawback of this material system is that the mobility in silicon is low. If a method for stacking several barriers is developed, this structure could be interesting for low-frequency, high-power applications. Another potential application for silicon based HBVs is voltage-variable tuning for integrated circuits.

3.3 Practical HBVs

This section provides an overview of HBV fabrication and the most common geometries utilised for HBVs.

3.3.1 Fabrication

The fabrication of HBV diodes essentially follows standard III-V processing techniques, see e. g. [59]. Details of the HBV fabrication at Chalmers can be found in [36].

3.3.2 Whisker-contacted geometries

The first HBVs where whisker-contacted [10]. Whisker-contacted HBVs have higher cut-off frequencies due to the low parasitics, but are less mechanically reliable than planar diodes and not suitable for integration. In order to improve the thermal properties of whisker-contacted HBVs, we introduced a process where the semiconductor substrate is replaced with copper, see Dillner *et al.* [60], [Paper G]. Compared to semiconductor substrates, copper has excellent thermal and electrical conductivities. In this process, the semiconductor substrate is replaced with copper before the devices are fabricated. First, a Ti/Pt/Au ohmic contact is evaporated onto the top layer. Then, copper is electroplated to a thickness of approximately 50 μm and covered with a thin layer of gold for chemical protection. The InP substrate is removed with a selective wet etch, where the InGaAs contact layer, see Table 3.2, serves as an etch stop layer. Now, the epitaxial layers are stacked on the copper substrate in reversed order compared to the growth order on the original InP substrate. This is possible because of the symmetric structure of HBV materials. Circular diode mesas are then fabricated using standard processing techniques. To facilitate whisker contacting of the diodes, it is advantageous to incorporate a whisker support at the top of the mesas. We have tried two different methods. The first is to form a Ti/Au "cup" on each mesa, see Figure 3.8 (left). This method gives a good ohmic contact between the whisker and the mesa, but the cups turned out to be too fragile, and difficult to contact because of the small size. The second method is to sputter SiO_2 on the diode chip, and wet-etch openings on each mesa, Figure 3.8 (right). This method gives a very good mechanical support for the whisker, but it is difficult to obtain a good ohmic contact, because after annealing, the top metal layer is an alloy and not pure gold. A solution to this problem is to deposit an additional layer of gold on top of the mesas after fabrication of the SiO_2 supports. Figure 3.9 shows a matrix

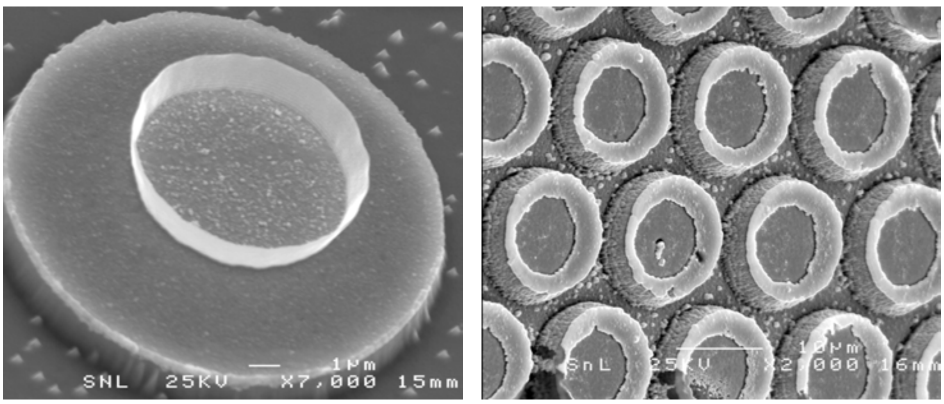

Figure 3.8: Chalmers whisker contacted HBVs on a copper substrate. Two approaches to whisker supports are shown, (left) a Ti/Au "cup" and (right) a SiO_2 "crater".

of whisker-contacted HBVs on a copper substrate in a frequency tripler.

Figure 3.9: Detail of a frequency tripler. A matrix of whisker-contacted HBVs on a copper substrate is soldered onto the wall of the output waveguide, and a planar whisker, soldered onto a gold-on-quartz filter, is connected to one of the diodes [35].

3.3.3 Planar geometries

Today, planar geometries [43, 61] are used almost exclusively for HBVs. Planar HBVs are easy to mount in frequency multiplier circuits, mechanically stable and reliable, and suitable for integration with other components. The symmetric two-mesa structure generally employed also cancels out any asymmetries in the epitaxial layer structure. The main drawbacks with planar diodes are the relatively complicated fabrication process, parasitic elements and the inherent problems associated with the effect of self-heating [62, 63]. The planar HBV geometry employed at Chalmers is schematically shown in Figure 3.10. This planar diode geometry includes two series-connected mesas, which means that an N-barrier material yields an $N \times 2$-barrier device. The length and width of the air-bridge fingers and the anode geometry are crucial parameters for the thermal properties [63]. Figure 3.11 shows examples of planar HBVs fabricated at Chalmers.

3.3.4 Pillar geometries

A pillar diode topology for HBVs was suggested and fabricated at Chalmers by Alderman *et al.* [64]. Here, the substrate is removed and copper pillars are electroplated on each side of the mesa. This kind of device is very difficult to fabricate, notably due to the thick resist layers needed for the electroplating of the $\sim 20\mu$m thick copper pillars. Due to various process-related problems all fabricated devices where short-circuited and therefore no RF characterisation could be performed. However, the methods devel-

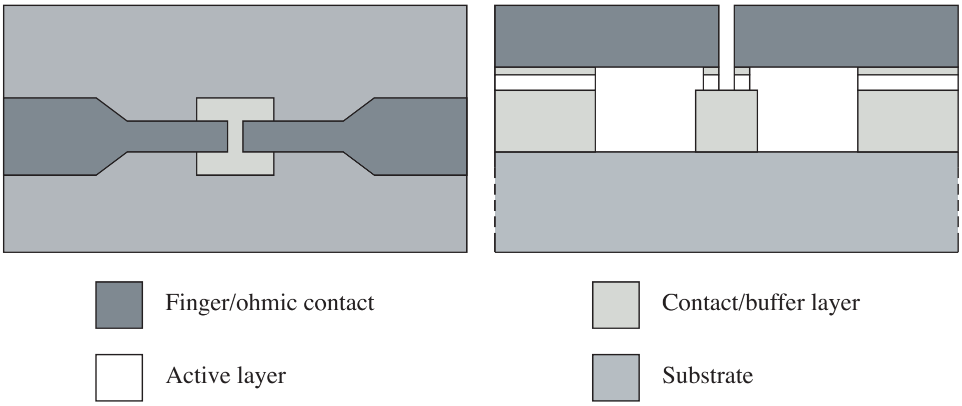

Figure 3.10: Top (left) and cross-sectional (right) schematic views of the planar HBV geometry used at Chalmers.

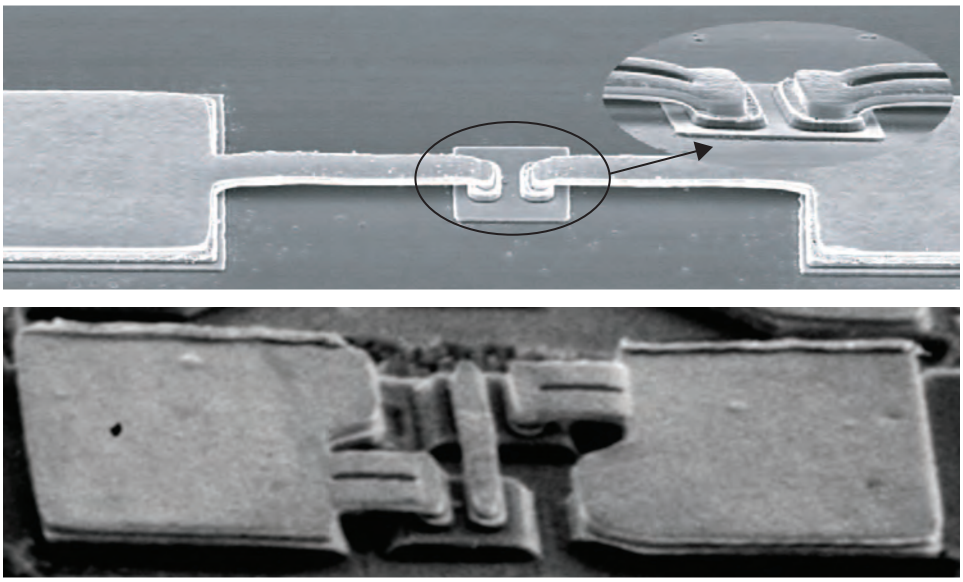

Figure 3.11: Planar HBVs fabricated at Chalmers. (Top) A device with two and (bottom) a device with four series-integrated mesas.

oped for using thick resist layers and for removing excessive semiconductor material during these experiments have been useful for process development of other device geometries. Figure 3.12 shows a pillar HBV soldered onto a gold-on-quartz filter.

Figure 3.12: Pillar HBV soldered onto a gold-on-quartz filter.

3.3.5 Integrated devices

Integrated topologies are often desirable as they offer easier mounting, better control and improved performance compared to discretes. A design with monolithically integrated low-pass filter, HBV diode and matching circuit has shown excellent performance [65]. Techniques, suitable for integration, for transferring HBVs to quartz substrates have been developed [66]. This transferring technique has resulted in HBVs monolithically integrated with a low-pass filter on a quartz substrate [67]. A possible, and indeed interesting, extension of these techniques could be to transfer HBVs to SiC or diamond substrates. Diamond and SiC have excellent thermal conductivities, which means that such substrates could serve as very good heat-sinks for planar HBVs. A less expensive alternative would be to use Si.

3.3.6 High-power devices

A multi-mesa HBV geometry designed to withstand very high power levels has been developed at Chalmers, see Figure 3.13 [68]. Here the absorbed power is distributed over a parallel connection of several series-connected mesa configurations. Compared to the conventional planar diode geometry, the peak temperature in device is reduced drastically.

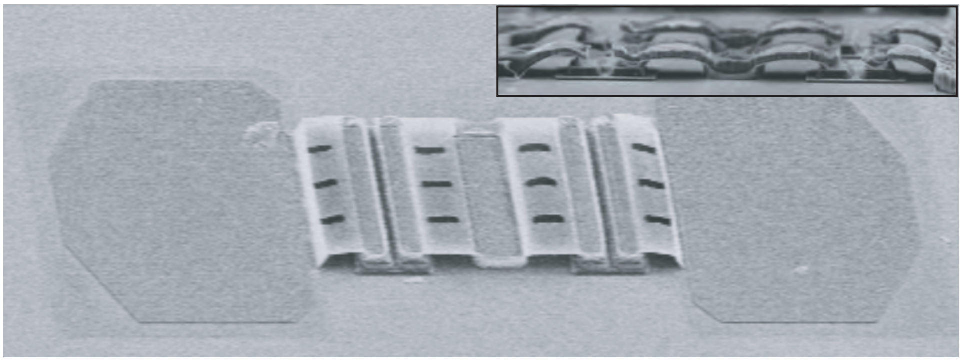

Figure 3.13: SEM picture of a high-power HBV with 16 5-barrier mesas, realised as four parallel connections of four series-integrated mesas. The inset shows a close-up of one row of four series-integrated mesas from a similar geometry, where the four parallel-connected parts are separated.

3.4 Thermal properties

As already mentioned, experimental results show that self-heating is a significant limiting factor for the performance of HBV frequency multipliers [62]. The term self-heating is used to describe the phenomenon that when the diode is pumped, the intrinsic device temperature increases, which results in an increased thermionic emission of electrons over the barrier. For GaAs-based devices, this increased leakage current typically reduces the conversion efficiency of frequency triplers from a theoretical value of 10-15% to approximately 3-5%. When the device temperature is increased, the series resistance increases whilst the maximum capacitance decreases, and this too has a negative effect on the conversion efficiency. InP-based HBVs are not as sensitive to self-heating effects as their GaAs counterparts, but suffer from the poor thermal conductivity of the InGaAs modulation layer, which results in very high peak temperatures in the diode mesa [Paper A]. In order to reduce the effect of self-heating, it is important to ensure that the thermal resistance of the HBVs is as low as possible. For planar devices, the air-bridge can be made shorter and with a larger cross-sectional area to reduce the thermal resistance. However, this increases the pad-to-pad capacitance. The geometry of the anodes also influences the thermal resistance. See [63], where the thermal resistance was reduced from about 2000 K/W to approximately 700 K/W by employing an improved diode geometry. It is possible to estimate the maximum allowable temperature for a given material system. For GaAs-based devices the main constraint is that the conduction current must be limited so as to ensure varactor mode operation of the HBV. For InP-based diodes, reliability studies [69, 70] give an indication of suitable allowable temperatures. By taking these constraints into consideration, we suggest a maximum allowable temperature of 420 K for both GaAs and InP-based devices [Paper A]. This temperature can then be used as a design parameter when optimising the thermal properties of HBVs, especially for high power applications [68].

3.4.1 Thermal estimations and models

3-D finite element (FEM) simulations are necessary to fully model and characterise the thermal properties of HBVs. Simple analytical expressions are, however, useful for initial estimations and comparisons between e. g. different material systems and device areas [Paper A]. The thermal resistance of a semiconductor mesa surrounded by air is given by

$$R_{\mathrm{th}} = \frac{L}{\kappa \cdot A}, \tag{3.19}$$

where L is the length and A is the cross-sectional area of the mesa, and κ is the thermal conductivity of the semiconductor material used. The one-dimensional steady state temperature profile throughout the mesa $T(x)$ can be calculated from the heat flow equation

$$\frac{\partial^2 T(x)}{\partial x^2} = -\frac{P_{\mathrm{tot}}}{LA\kappa}. \tag{3.20}$$

Here a homogenously distributed heat source is assumed, and P_{tot} is the total power absorbed in the mesa. The solution to (3.20) and a discussion about the results that can be obtained are given in [Paper A].

3.5 Design of HBV layer structures

An advantage with HBVs is that it is possible to tailor the devices for different applications. For sub-millimetre wave applications, the main goal is to maximise the conversion efficiency for a given input frequency, input power level and multiplication factor. This is closely related to maximising the cut-off frequency, (2.3). At lower frequencies, higher input power levels are available, and the HBV must also be optimised with respect to power handling capacity. Optimisation of the power handling capability involves maximising the breakdown voltage of the device. This section presents a method for optimising the cut-off frequency, based on the work by Crowe *et al.* for Schottky diodes [26]. However, for terahertz operation, the current saturation effect must be taken into account [25]. The design goal is, then, to optimise the cut-off frequency with the current saturation effect as an optimisation constraint. The optimum layer structure depends on the input power level and the diode geometry, since the series resistance depends on the diode geometry and the number of barriers. For a given diode geometry, the design procedure is as follows.

1. Choose **material system**, e.g. GaAs/$\mathrm{Al_xGa_{1-x}As}$ on GaAs or $\mathrm{In_xGa_{1-x}As/Al_yIn_{1-y}As}$ on InP.

2. Estimate the **number of barriers** and the **device area** needed to handle the input power [16].

3. Calculate the **thickness of the modulation layers**, l_{max} . Current saturation limits the maximum thickness to

$$l_{\mathrm{max}} = \frac{v_{\mathrm{sat}}}{4kf_{\mathrm{p}}} \tag{3.21}$$

   where v_{sat} is the saturated electron velocity, k is the ratio between v_{sat} and the average electron speed during a half pump cycle [16] and f_{p} is the pump frequency. For HBV triplers, $k \approx 2$. The modulation layers should be thick enough to accommodate the full depletion layer thickness at the maximum voltage during frequency multiplier operation. Thicker layers will add extra series resistance, whilst thinner layers reduce the elastance modulation ratio.

4. Choose the **doping concentration** for the modulation layers. In order to minimise the series resistance, the modulation layers are usually doped as heavily as possible, but not higher than that the modulation layers can be fully depleted without exceeding the avalanche breakdown voltage. A rough estimation of the breakdown voltage can be derived from the well-known breakdown voltage expression for an abrupt PN-junction [71]

$$V_{\mathrm{BD}} = 60\left(\frac{E_{\mathrm{g}}}{1.1}\right)^{3/2}\left(\frac{N_{\mathrm{D}}}{10^{16}}\right)^{-3/4} \tag{3.22}$$

   where E_{g} is the band-gap at room temperature in eV and N_{D} is the doping concentration in $\mathrm{cm^{-3}}$. Equation (3.22) is accurate for many semiconductors including GaAs, but does not seem be trustworthy for InGaAs. We use modified versions of (3.22), fitted to breakdown voltage measurements on InP-based HBV materials. The modulation layer thickness l is obtained by inserting (3.22) into

$$l = w_{\mathrm{max}} = \sqrt{\frac{2\varepsilon_{\mathrm{d}} V_{\mathrm{BD}}}{qN_{\mathrm{d}}}} \tag{3.23}$$

   where ε_{d} is the relative permittivity of the modulation layer material and q is the elementary charge.

5. When a high frequency multiplier conversion efficiency is needed, the **dynamic cut-off frequency** has to be maximised. This involves chosing a layer structure and doping concentration that maximise the elastance swing and minimise the series resistance.

6. Choose the **thickness of the barrier(s)** to minimise the leakage current [32] whilst still allowing for a high dynamic cut-off frequency.

7. **Optimise the design** with a harmonic balance simulator, using an appropriate voltage-charge relationship, (3.9), and a series resistance estimated from material data and contact resistance measurements.

8. **Check** that the available input power can be absorbed without exceeding the device breakdown voltage, optimum embedding impedance levels are achievable, and the device temperature is below the maximum allowable value. If not, iterate as appropriate by repeating the design procedure with a different number of barriers and/or a different device area.

More detailed information on the design of HBVs can be found in [16] and [Paper B].

Chapter 4

HBV frequency multipliers

A two-terminal frequency multiplier uses a nonlinear device that generates harmonics of the input frequency applied from a source. The nonlinear device can be either a nonlinear resistor, varistor, or a nonlinear reactance, varactor. Varistor multipliers have a potentially large intrinsic bandwidth due to the absence of stored reactive energy, but the conversion efficiency is limited to $1/n^2$, where n is the order of multiplication [72, 73]. Varactor multipliers, on the other hand, have a theoretical conversion efficiency in the ideal, loss-less case, of 100%, but have a narrow bandwidth and are very sensitive to the operating conditions. Due to the low available power levels in the millimetre and sub-millimetre regions, varactors are used exclusively at these frequencies. However, practical varactors such as HBVs exhibit properties that are a mixture of those of pure varistors and varactors, respectively. This section reviews basic design concepts for HBV multipliers and presents an overview of HBV multiplier cicuit topologies, performance, and measurement techniques.

4.1 Design of HBV multipliers

The design and analysis of frequency multipliers is an extensive topic. This section focuses on basic properties and device-related design issues, i. e. optimum impedance levels given certain device characteristics, or vice versa. Figure 4.1 shows the two possible basic forms for a single-HBV frequency multiplier, namely with the diode mounted either in shunt or series with respect to the input and output networks. The matching networks should be designed to provide optimum embedding impedances to the diode at the input and output frequency, respectively. Referring to Figure 4.1, in the shunt connected topology, the input matching network should present $\Gamma_S = 1$ (i. e. an open circuit) to the output frequency whilst the output matching network should provide $\Gamma_L = 1$ at the fundamental frequency. For the series mounted case the opposite conditions must be fulfilled, i. e.

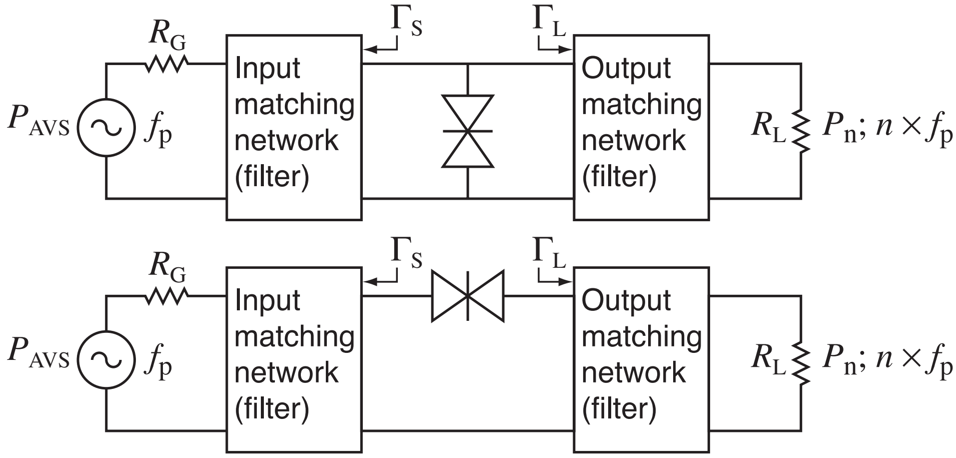

Figure 4.1: Schematic block representation of an nth-order frequency multiplier circuit with (top) shunt-mounted and (bottom) series-mounted diode.

$\Gamma_S = -1$ for $f = n \times f_0$ and $\Gamma_L = -1$ for $f = f_0$, i. e. short circuits. For HBV multipliers with $n > 3$ the matching networks must also provide appropriate idler circuits. An HBV quintupler ($n = 5$) for example needs an idler circuit for the third harmonic, $3 \times f_0$, in order to maximise the conversion efficiency to the fifth harmonic. There are two extreme cases for the realisation of the idler circuit, here represented by the idler impedance Z_3, for a quintupler:

1. Zero current flowing at $3 \times f_0$, i. e. $Z_3 = \infty$. The third harmonic will thus not cause any losses.

2. Maximise the current at $3 \times f_0$. This can be achieved by providing an inductance in resonance with the diode capacitance at $3 \times f_0$. That is, $Z_3 = jX_3$, where $S_{min}/3\omega_p < X_3 < S_{max}/3\omega_p$. This way the idler current, in combination with the input signal, will increase the output power, but also introduce losses in the series resistance.

4.1.1 Optimum impedance levels

For frequency multipliers, *optimum impedances* means impedances that, if presented to the diode, maximise the conversion efficiency from f_0 to $n \times f_0$. The optimum impedances are denoted e. g. $Z_{S,opt}$ and $Z_{L,opt}$, respectively, and depend mutually on each other and on the input power level. However, generally, impedances are only defined for linear networks. Therefore, a quasi impedance Z_n is defined at harmonic n of a periodic signal as

$$Z_n = \frac{V_n}{I_n}, \tag{4.1}$$

where V_n and I_n are the voltage and current, respectively, at harmonic n. In order to maximise the power transfer, the matching network impedance should be conjugate matched to device impedance. One analytical approach is to use the the cubic voltage-charge relation of (2.10). Then,the input and output impedances for optimum conversion efficiency can be approximated by the following empirical expressions [74] :

$$Z_{\mathrm{in}} = \frac{(k_1 - \mathrm{j}k_2)(S_{\mathrm{max}} - S_{\mathrm{min}}) - \mathrm{j}S_{\mathrm{min}}}{\omega_{\mathrm{p}}} + (k_3 - \mathrm{j}k_4)R_{\mathrm{s}} \tag{4.2}$$

and

$$Z_{\mathrm{n}} = \frac{(k_1 + \mathrm{j}k_2)(S_{\mathrm{max}} - S_{\mathrm{min}}) + \mathrm{j}S_{\mathrm{min}}}{n \cdot \omega_{\mathrm{p}}} + (k_3 + \mathrm{j}k_4)R_{\mathrm{s}}, \tag{4.3}$$

where ω_{p} is the angular pump or input frequency. The constants k_{n} are given in Table 4.1 for the cubic capacitance model. For $f_{\mathrm{p}}/f_{\mathrm{c}} \ll 1$, k_3 and k_4 can be neglected.

Table 4.1: Coefficients for optimum tripler and quintupler impedances for the cubic model.

n		k_1	k_2	k_3	k_4
3	Z_{in}	0.046	0.21	0.78	0.25
	Z_3	0.28	0.35	0.55	0.08
5	Z_{in}	0.057	0.19	0.88	0.27
	Z_3	0	0.35	0	0.29
	Z_5	0.26	0.24	0.62	0.22

Load-pull simulations

Load-pull simulations are very useful for investigating impedance levels and their dependence on various parameters. To this end, we use Chalmers HBV model, (3.9), (3.10) or (3.12), and (3.14), implemented in the commercial software Microwave Office. Harmonic balance simulations are used to determine the optimum impedance levels. The result in the form of conversion loss contours from simulations of a 500 GHz HBV quintupler is shown in Figure 4.2. When Z_1 is swept over the entire Smith chart, Z_3 and Z_5 are fixed at their respective optimum levels, and so forth. It is obvious that the input matching is very crucial.

4.1.2 Noise in varactor multipliers

Being a mainly reactive device, a varactor generates very little noise. Thermal noise generated by the series resistance at all frequencies present is

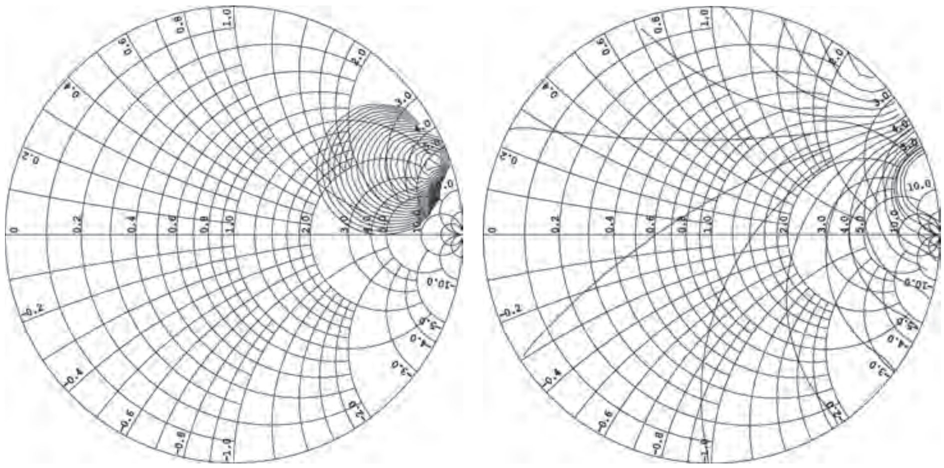

Figure 4.2: Conversion loss contours versus (left) input and (right) idler impedance. The results are obtained from harmonic balance simulations of a 500 GHz quintupler. The device assumed is a 2×3-barrier InP-based planar HBV with an area of 37 μm^2. The minimum conversion loss is 5.1 dB and the contours correspond to an increase in conversion loss of 1 dB.

generally the dominating noise source in varactor multipliers [75]. As a consequence, in an application where the noise performance is important, it is necessary to eliminate the current flowing at idler frequencies. The thermal noise generated in a bandwidth Δf around a certain frequency can be represented by the rms value of the noise voltage $v_{\mathrm{n,rms}}$:

$$v_{\mathrm{n,rms}} = \sqrt{4kTR_{\mathrm{s}}\Delta f} \tag{4.4}$$

where k is the Boltzmann constant and T is the device temperature. A frequency multiplier also multiplies phase, the phase noise is degraded by n^2, where n is the multiplication factor [13, 75]. No phase noise measurements have yet been reported for HBVs.

4.2 HBV tripler and quintupler topologies

The vast majority of HBV multipliers this far have been frequency triplers. Today the focus is directed towards higher frequencies, and therefore the interest for higher order multipliers, notably quintuplers, is increasing. It is also possible to use HBVs for generating even harmonics by applying a DC bias that makes the energy band structure asymmetric. A few HBV frequency doublers have been fabricated and tested, but nothing has been published. The potential advantage of using HBVs rather than Schottky diodes for frequency doubling is the higher power handling capacity offered by a multi-barrier HBV. Triplers and quintuplers basically use the same kind of circuit topologies, the most commonly utilised of these are described in this section.

4.2.1 Crossed waveguide multipliers

The most common multiplier configuration for millimetre and sub-millimetre wave applications is the crossed waveguide configuration. The circuit consists of a metal block with waveguides for the input and output signals, see Figure 4.3. The widths of the waveguides correspond to the input frequency f_p and the output frequency $n \times f_\mathrm{p}$, respectively. In the output waveguide, the input frequency is cut-off, which means that the waveguide acts as a high-pass filter, thus preventing power at f_p from propagating to the output of the multiplier. The pump power at f_p is coupled to the output waveguide through a probe, which protrudes into the input waveguide. The probe is integrated with a low-pass filter, which prevents power at $n \times f_\mathrm{p}$ leaking out to the input. Usually, the low-pass filter with the probe is made of gold-on-quartz in a high-low impedance configuration. In order to provide the HBV with suitable embedding impedances, it is common to include moveable shorts in the input and output waveguide sections, usually one E-plane tuner and one backshort. The input tuners are shown in Figure 4.3. The HBV, which is of a planar geometry in the circuit of Figure 4.3, is soldered with one pad on to the end of the low-pass filter, and the other pad on to the waveguide block. Waveguides exhibit low losses, although the moveable shorts introduce some losses in a multiplier circuit.

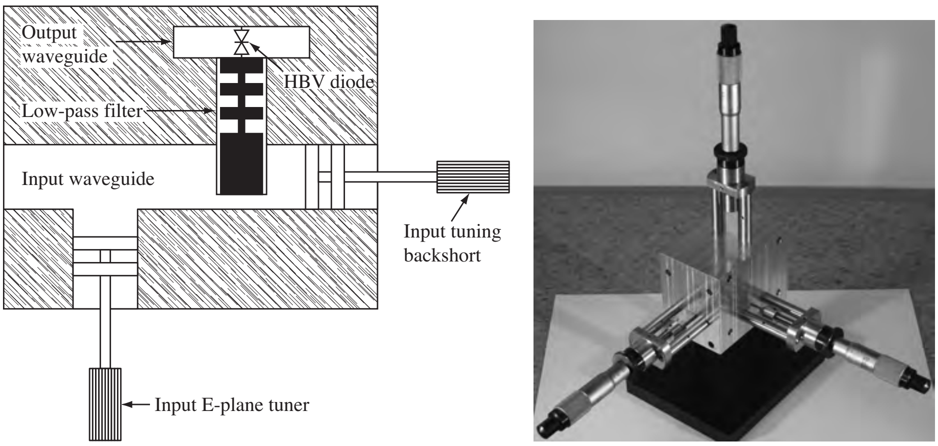

Figure 4.3: (Left) cross section of a crossed waveguide frequency multiplier and (right) photo of a 100-GHz HBV quintupler with two input tuners and one output tuner.

4.2.2 Distributed multipliers

Another approach to the realisation of HBV frequency triplers is to use nonlinear transmission lines (NLTLs). NLTLs offer high bandwidths. The main drawbacks are that the peak efficiency is lower than for single device multipliers, and that the mounting procedure is complex. To simplify the analysis and design, it is preferable to use a linear transmission line, periodically loaded with nonlinear devices, rather than using a fully distributed NLTL. The first demonstration of an NLTL HBV tripler was performed by Hollung *et al.* at Chalmers [76]. This tripler consists of a finline, periodically loaded with 15 HBVs, see Figure 4.4. The finline configuration is possible to use, as HBVs do not need any DC bias. Propagation of the incident wave through the nonlinear transmission line generates the third harmonic, which is radiated into free space from a tapered slot antenna at the output. Recently, a broadband integrated HBV tripler using a nonlinear transmission line topology with six HBVs was presented [77]. Here, HBVs and finline transitions are integrated on a low-loss membrane to reduce parasitics and enable output frequencies up to 600 GHz.

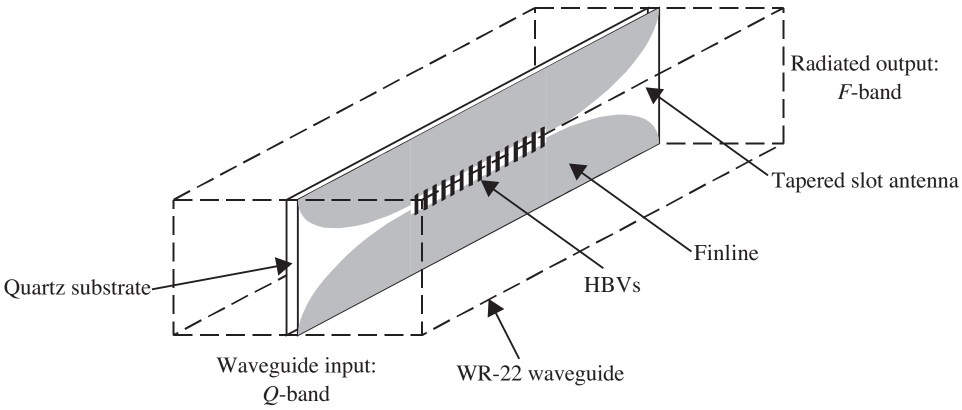

Figure 4.4: A distributed HBV frequency tripler [76].

4.2.3 Waveguide-integrated microstrip multipliers

At Chalmers we have developed a new HBV multiplier topology where the HBV is embedded in a microstrip environment together with parts of the matching network, see Olsen *et al.*, [78]. The topology is suitable for both triplers [Paper F] and quintuplers [Paper E]. The circuit is mounted in a rectangular waveguide and e. g. antipodal finline tapers can be used as transitions between the waveguide and the microstrip circuit. A tripler version of this circuit topology is shown in Figure 4.5. Figure 4.6 shows a photo of a 100-GHz waveguide-integrated microstrip quintupler [Paper E].

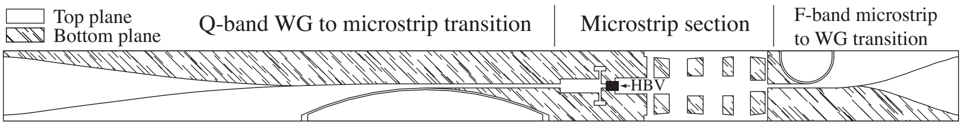

Figure 4.5: A waveguide-integrated microstrip HBV tripler with antipodal finline transitions and microstrip embedding circuit.

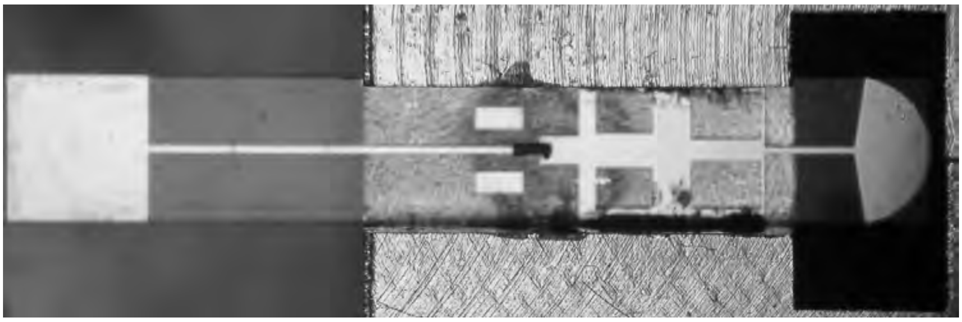

Figure 4.6: Detail of a 100-GHz HBV waveguide-integrated microstrip quintupler. The gold-on-quartz circuit is mounted in a channel between the input (left) and output (right) waveguides [Paper E].

4.2.4 Quasi-optical multipliers

Quasi-optical circuits are well suited for high-frequency applications, especially the upper sub-millimetre wave region, where the losses in waveguide circuits are higher and affect the performance noticeably. Decreasing dimensions also complicate the machining of waveguide circuits at these frequencies. Figure 4.7 shows a quasi-optical HBV frequency tripler, where two slot antennas loaded with HBVs are located at the focal plane of a dielectric lens [79].

4.3 Frequency multiplier measurements

4.3.1 Measurements on waveguide multipliers

Hitherto, most HBV circuits have been triplers designed to operate at input frequencies in the W-band, 75-110 GHz. The two main constraints when choosing frequency bands for multiplier design, in terms of characterisation possibilities, are (i) the availability of fundamental power sources and (ii) the availability of power measurement devices. At W-band, Gunn oscillators and backward-wave oscillators (BWOs) can produce power levels of about 100 mW, or 20 dBm. A typical measurement set-up is schematically shown in Figure 4.8, whilst Figure 4.9 shows a photo of such a set-up for HBV waveguide quintupler measurements. Figure 4.10 shows results from measurements on a typical HBV tripler.

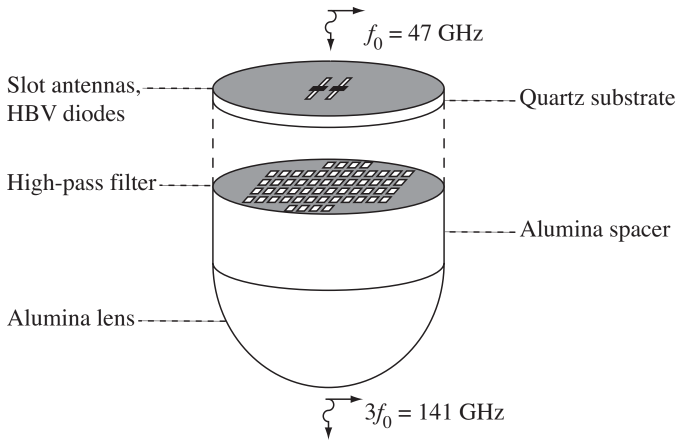

Figure 4.7: A quasi-optical HBV frequency tripler [79].

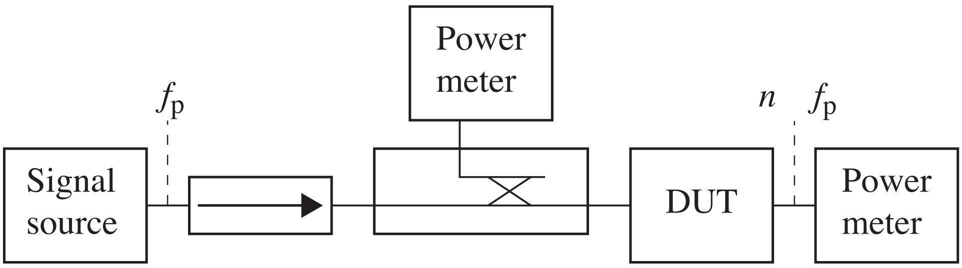

Figure 4.8: Schematical representation of a typical measurement set-up for waveguide multiplier measurements.

Figure 4.9: Photo of a measurement set-up for a waveguide circuit, showing power meters, signal synthesiser with an amplifier, waveguide block with moveable tuners and directional coupler.

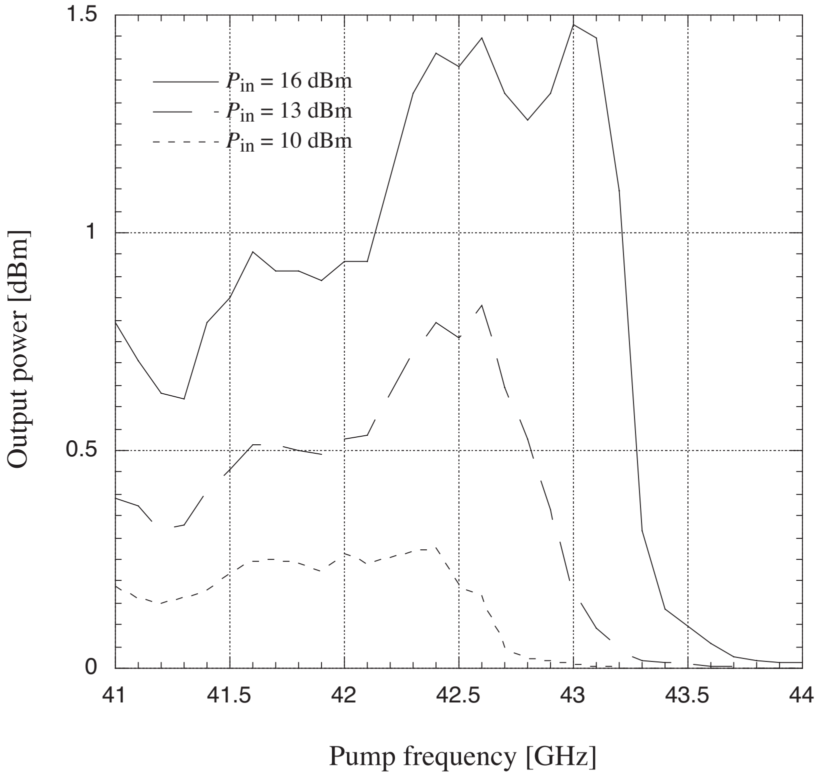

Figure 4.10: Output power versus pump frequency for an F-band HBV frequency tripler for three different levels of input power.

4.3.2 Cooled measurements

Results from cooled measurements are useful for evaluating the thermal properties of HBV device geometries. The performance obtained from measurements on HBV multipliers at room temperature can be compared to the results obtained at cooled temperatures. Well-designed diodes should show less difference in efficiencies at different temperatures, cf [35, 62]. Cooled measurements are performed in a vacuum environment inside a cryostat. A problem, then, is that when the circuit is mounted inside the cryostat, it is not possible to perform any tuning of the circuit. This problem can be solved by using a computer-controlled system, where the computer performs the impedance matching of the circuit with stepper motors. The stepper motors are connected to drive shafts, which penetrate the walls of the cryostat through vacuum feed-throughs, and are connected to moveable tuners on the circuit [80]. Figure 4.11 (left) shows a photograph of such a cryostat with the top lid removed and an HBV tripler mounted on the 20 K stage. The computer-controlled system can also be used for circuit characterisation at room temperature. An example is shown in Figure 4.11 (right). A cooled

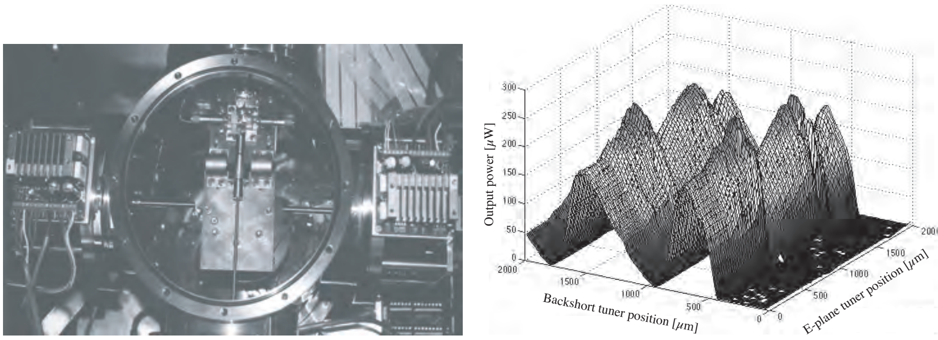

Figure 4.11: (Left) photo of a cryostat equipped with stepper motors, allowing for computer-controlled impedance matching and measurements. (Right) output power versus position of the output tuners from an HBV tripler, measured with the computer-controlled system [80].

measurement performed in the cryostat of Figure 4.11 is shown in Figure 4.12.

4.4 HBV multiplier performance

Table 4.2 summarises the state-of-the-art for HBV triplers and quintuplers at various frequencies. The results presented are also visualised in Figure 4.13.

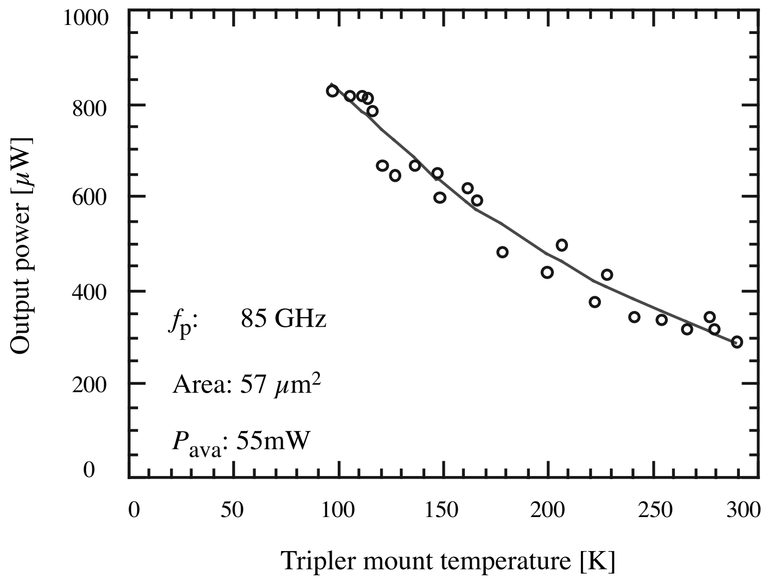

Figure 4.12: Measured output power versus mount temperature for an HBV tripler with a 2×2-barrier GaAs-based diode [62].

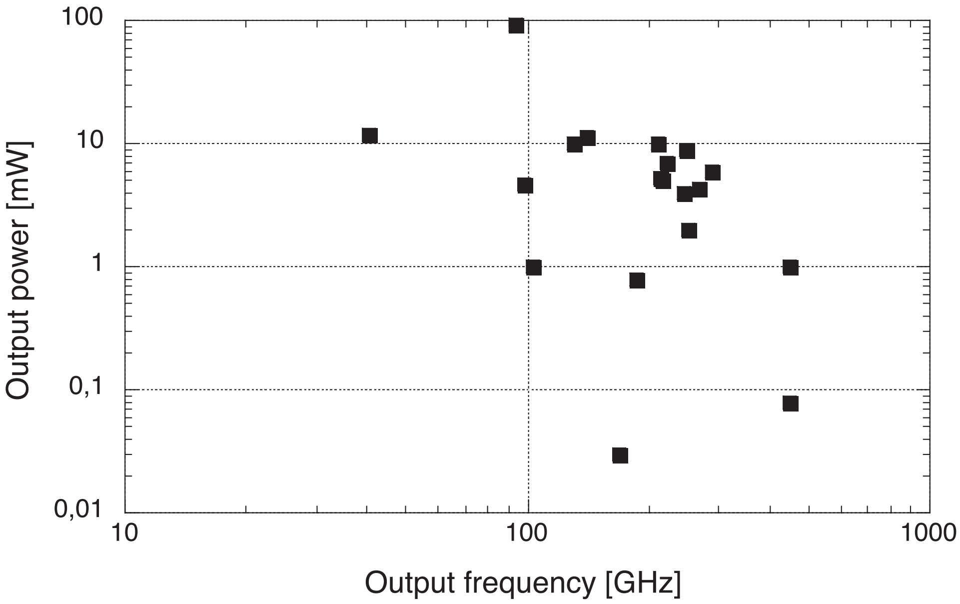

Figure 4.13: Output power versus output frequency for the HBV multipliers summarised in Table 4.2.

Table 4.2: HBV multiplier performance.

f [GHz]	η [%]	P_{out} [mW]	N	Sub.	Ref.	Comment
3×13.5	7.6	12	3	InP	[81]	
3×31	10	91	10	InP	[48]	
3×33	0.7	1250	3	GaAs	[82]	Quasi-optical
3×43.5	7	10	4	GaAs	[76]	NLTL
3×47	8	11.5	4	GaAs	[79]	Quasi-optical
3×62	2	0.8	1	GaAs	[83]	
3×70	13.5	10	1	GaAs	[65]	
3×72	5.4	5	4	InP	[20]	
3×74	7.9	7.1	3	Cu	[35]	
3×82	4.8	4	4	GaAs	[63]	
3×82.5	12	9	4	InP	[84]	
3×84	2.5	2	4	GaAs	[43]	
3×89	5.6	4.3	3	Cu	[19]	
3×96	6	6	6	Quartz	[67]	
3×150	0.05	0.08	2	Au	[23]	
3×150	1.5	1	4	GaAs	[85]	
5×19.7	11.4	4.6	4	InP	[Paper D]	
5×20.5	4.9	1.0	4	GaAs	[Paper E]	
5×34	0.78	0.03	1	InP	[86]	
5×42.5	5.2	5.2	4	InP	[87]	

Chapter 5

Summary of appended papers

Paper A presents an analytical model for the temperature profile throughout an HBV.

Paper B deals with device-level design of high frequency HBV multipliers, exemplified by a 500 GHz quintupler design.

Paper C presents an electro-thermal HBV model for harmonic balance analysis including self-heating effects.

Paper D presents world-record results for HBV quintuplers.

Paper E describes a 100 GHz HBV quintupler.

Paper F presents an F-band HBV tripler.

Paper G describes the fabrication of HBVs on copper substrates.

References

[1] P. H. Siegel, "Terahertz technology in biology and medicine," *IEEE Transactions on Microwave Theory and Techniques*, vol. 52, no. 10, pp. 2438–2447, 2004.

[2] R. Köhler, A. Tredicucci, F. Beltram, H. E. Beere, E. H. Linfield, A. G. Davies, D. A. Ritchie, R. C. Iotti, and F. Rossi, "Terahertz semiconductor-heterostructure laser," *Nature*, vol. 417, pp. 156–159, 2002.

[3] B. S. Williams, H. Callebaut, S. Kumar, Q. Hu, and J. L. Reno, "3.4-THz quantum cascade laser based on longitudinal-optical-phonon scattering for depopulation," *Applied Physics Letters*, vol. 82, no. 7, pp. 1015–1017, 2003.

[4] B. S. Williams, S. Kumar, H. Callebaut, Q. Hu, and J. L. Reno, "Terahertz quantum-cascade laser at $\lambda \approx 100\mu$m using metal waveguide for mode confinement," *Applied Physics Letters*, vol. 83, no. 11, pp. 2124–2126, 2003.

[5] S. C. Lee and A. Wacker, "Theoretical analysis of spectral gain in a terahertz quantum-cascade laser: Prospects for gain at 1 THz," *Applied Physics Letters*, vol. 83, no. 13, pp. 2506–2508, 2003.

[6] E. Peytavit, S. Arscott, D. Lippens, G. Mouret, S. Matton, P. Masselin, R. Bocquet, J. F. Lampin, L. Desplanque, and F. Mollot, "Terahertz frequency difference from vertically integrated low-temperature-grown GaAs photodetector," *Applied Physics Letters*, vol. 81, no. 7, pp. 1174–1176, 2002.

[7] H. Ito, T. Nagatsuma, A. Hirata, T. Minotani, A. Sasaki, Y. Hirota, and T. Ishibashi, "High-power photonic millimetre wave generation at 100 GHz using matching-circuit-integrated uni-travelling-carrier photodiodes," *IEE Proceedings Optoelectronics*, vol. 150, no. 2, pp. 138–142, 2003.

[8] T. Crowe, R. Mattauch, H. Roser, W. Bishop, W. Peatman, and X. Liu, "GaAs Schottky diodes for THz mixing applications," *Proceedings of the IEEE*, vol. 80, no. 11, pp. 1827–1841, 1992.

[9] N. R. Erickson, R. M. Grosslein, J. Wielgus, and V. Fath, "A 1650-1900 GHz tunable source," in *Proceedings of the 14th International Symposium on Space Terahertz Technology*, 2003, pp. 64–72.

[10] E. L. Kollberg and A. Rydberg, "Quantum-barrier-varactor diodes for high-efficiency millimetre-wave multipliers," *Electronics Letters*, vol. 25, no. 25, pp. 1696–1698, 1989.

[11] P. Penfield and R. P. Rafuse, *Varactor Applications.* Cambridge: M.I.T. Press, 1962.

[12] J. Stake, *The RF and microwave handbook.* CRC Press LLC, 2001, ch. Varactors.

[13] M. T. Faber, J. Chramiec, and M. E. Adamski, *Microwave and Millimeter-Wave Diode Frequency Multipliers.* Artech House, 1995.

[14] J. W. Manley and H. E. Rowe, "Some general properties of nonlinear elements," *Institute of Radio Engineers - Proceedings*, vol. 44, no. 7, pp. 904–913, 1956.

[15] L. Dillner, J. Stake, and E. L. Kollberg, "Analysis of symmetric varactor frequency multipliers," *Microwave and Optical Technology Letters*, vol. 15, no. 1, pp. 26–29, 1997.

[16] J. Stake, S. H. Jones, L. Dillner, S. Hollung, and E. L. Kollberg, "Heterostructure-barrier-varactor design," *IEEE Transactions on Microwave Theory and Techniques*, vol. 48, no. 4, pp. 677 – 682, 2000.

[17] K. Krishnamurthi and R. G. Harrison, "Analysis of symmetric-varactor frequency triplers," in *IEEE MTT-S International Microwave Symposium Digest*, 1993, pp. 649–652.

[18] C. H. Tang, "An exact analysis of varactor frequency multipliers," *IEEE Transactions on Microwave Theory and Techniques*, vol. 14, no. 4, pp. 210–212, 1966.

[19] L. Dillner, "Heterostructure barrier varactors for high efficiency frequency multipliers," Ph.D. dissertation, Chalmers University of Technology, 2000.

[20] X. Melique, C. Mann, P. Mounaix, J. Thornton, O. Vanbesien, F. Mollot, and D. Lippens, "5-mW and 5% efficiency 216-GHz InP-based heterostructure barrier varactor tripler," *IEEE Microwave and Guided Wave Letters*, vol. 8, no. 11, pp. 384–386, 1998.

[21] X. Mélique, A. Maestrini, R. Farré, P. Mounaix, M. Favreau, O. Vanbésien, J. M. Goutoule, F. Mollot, G. Beaudin, T. Nähri, and D. Lippens, "Fabrication and performance of InP-based heterostructure barrier varactors in a 250 GHz waveguide tripler," *IEEE Transactions on Microwave Theory and Techniques*, vol. 48, no. 6, pp. 1000–1006, 2000.

[22] L. Dillner, S. Hollung, M. Ingvarson, E. Kollberg, W. Strupinski, C. Mann, and J. Stake, "High efficiency HBV multipliers for millimeter wave generation," in *Proceedings of the 13th International Conference on Microwaves, Radar and Wireless Communications*, 2000, pp. 47–54.

[23] M. Saglam, B. Schumann, V. Mullerwiebus, A. Megej, U. Auer, M. Rodriguez-Girones, R. Judaschke, E. Tegude, and H. Hartnagel, "450 GHz millimetre-wave signal from frequency tripler with heterostructure barrier varactors on gold substrate," *Electronics Letters*, vol. 38, no. 13, pp. 657–658, 2002.

[24] Y. Fu, M. Mamor, M. Willander, S. Bengtsson, and L. Dillner, "*n*-Si/SiO_2/Si heterostructure barrier varactor diode design," *Applied Physics Letters*, vol. 77, no. 1, pp. 103–105, 2000.

[25] E. L. Kolberg, T. J. Tolmunen, M. A. Frerking, and J. R. East, "Current saturation in submillimeter-wave varactors," *IEEE Transactions on Microwave Theory and Techniques*, vol. 40, no. 5, pp. 831 – 838, 1992.

[26] T. W. Crowe, T. C. Grein, R. Zimmermann, and P. Zimmermann, "Progress toward solid-state local oscillators at 1 THz," *IEEE Microwave and Guided Wave Letters*, vol. 6, no. 5, pp. 207–208, 1996.

[27] J. Stake and H. Grönqvist, "An on-wafer method for C-V characterisation of heterostructure diodes," *Microwave and Optical Technology Letters*, vol. 9, no. 2, pp. 63–66, 1995.

[28] J. Stake, L. Dillner, S. H. Jones, E. L. Kollberg, and C. M. Mann, "Design of 100-900 GHz AlGaAs/GaAs planar heterostructure barrier varactor frequency triplers," in *Proceedings of the 9th International Symposium on Space Terahertz Technology*, 1998, pp. 359–366.

[29] L. Dillner, J. Stake, and E. L. Kollberg, "Modeling of the heterostructure barrier varactor diode," in *Proceedings of the 1997 International Semiconductor Device Research Symposium*, 1997, pp. 179–182.

[30] H. Hjelmgren, "Numerical modelling of hot electron transport in Schottky-diodes and heterojunction structures," Ph.D. dissertation, Chalmers University of Technology, 1991.

[31] J. R. Jones, S. H. Jones, G. B. Tait, and M. F. Zybura, "Heterostructure barrier varactor simulation using an integrated hydrodynamic device/harmonic-balance circuit analysis technique," *IEEE Microwave and Guided Wave Letters*, vol. 4, no. 12, pp. 411–413, 1994.

[32] Y. Fu, J. Stake, L. Dillner, M. Willander, and E. L. Kollberg, "AlGaAs/GaAs and InAlAs/InGaAs heterostructure barrier varactors," *Journal of Applied Physics*, vol. 82, no. 11, pp. 5568–5572, 1997.

[33] E. Lheurette, P. Mounaix, P. Salzenstein, F. Mollot, and D. Lippens, "High performance InP-based heterostructure barrier varactors in single and stack configuration," *Electronics Letters*, vol. 32, no. 15, pp. 1417–1418, 1996.

[34] Y. Fu, J. Stake, L. Dillner, M. Willander, and E. L. Kollberg, "Carrier conduction in a heterostructure barrier varactor induced by an ac-bias," *Superlattices and Microstructures*, vol. 28, no. 2, pp. 135–141, 2000.

[35] L. Dillner, W. Strupinski, S. Hollung, C. Mann, J. Stake, M. Beardsley, and E. Kollberg, "Frequency multiplier measurements on heterostructure barrier varactors on a copper substrate," *IEEE Electron Device Letters*, vol. 21, no. 5, pp. 206 – 208, 2000.

[36] J. Stake, L. Dillner, and M. Ingvarson, "Fabrication and characterisation of heterostructure barrier varactor diodes," Chalmers University of Technology, Tech. Rep. 29, 1996.

[37] L. E. Dickens, "Spreading resistance as a function of frequency," *IEEE Transactions on Microwave Theory and Techniques*, vol. 15, no. 2, pp. 101–109, 1967.

[38] M. Sotoodeh, A. H. Khalid, and A. A. Rezazadeh, "Empirical low-field mobility model for III–V compounds applicable in device simulation codes," *Journal of Applied Physics*, vol. 87, no. 6, pp. 2890–2900, 2000.

[39] J. R. Jones, S. H. Jones, and G. B. Tait, "Self-consistent physics-based numerical device/harmonic-balance circuit analysis of heterostructure barrier varactors including thermal effects," in *Proceedings of the 6th International Symposium on Space Terahertz Technology*, 1995, pp. 423–441.

[40] J. R. Jones, G. Tait, S. Jones, and D. Katzer, "DC and large-signal time-dependent electron transport in heterostructure devices: an investigation of the heterostructure barrier varactor," *IEEE Transactions on Electron Devices*, vol. 42, no. 8, pp. 1393–1403, 1995.

[41] J. Stake, S. H. Jones, J. R. Jones, and L. Dillner, “Analysis of carrier transport in a heterostructure barrier varactor diode tripler,” in *Proceedings of the 1997 International Semiconductor Device Research Symposium*, 1997, pp. 183–186.

[42] R. E. Lipsey, S. H. Jones, J. R. Jones, T. W. Crowe, L. F. Horvath, U. V. Bhapkar, and R. J. Mattauch, “Monte Carlo harmonic-balance and drift-diffusion harmonic-balance analyses of 100-600 GHz Schottky barrier varactor frequency multipliers,” *IEEE Transactions on Electron Devices*, vol. 44, no. 11, pp. 1843–1850, 1997.

[43] J. R. Jones, W. L. Bishop, S. H. Jones, and G. B. Tait, “Planar multibarrier 80/240-GHz heterostructure barrier varactor triplers,” *IEEE Transactions on microwave theory and techniques*, vol. 45, no. 4, pp. 512–518, 1997.

[44] K. Krishnamurthi, S. M. Nilsen, and R. G. Harrison, “GaAs single-barrier varactors for millimeter-wave triplers: guidelines for enhanced performance,” *IEEE Transactions on Microwave Theory and Techniques*, vol. 42, no. 12, pp. 2512 – 2516, 1994.

[45] J. R. Jones, S. H. Jones, and G. B. Tait, “GaAs/InGaAs/AlGaAs heterostructure barrier varactors for frequency tripling,” in *Proceedings of the 5th International Symposium on Space Terahertz Technology*, 1994, pp. 497–513.

[46] V. Duez, X. Mélique, O. Vanbésien, P. Mounaix, F. Mollot, and D. Lippens, “High capacitance ratio with GaAs/InGaAs/AlAs heterostructure quantum well-barrier varactors,” *Electronics Letters*, vol. 34, no. 19, pp. 1860 – 1861, 1998.

[47] V. K. Reddy and D. P. Neikirk, “High breakdown voltage AlAs/InGaAs quantum barrier varactor diodes,” *Electronics Letters*, vol. 29, no. 5, pp. 464 – 466, 1993.

[48] A. Rahal, R. G. Bosisio, C. Rogers, J. Ovey, M. Sawan, and M. Missous, “A W-band medium power multi-stack quantum barrier varactor frequency tripler,” *IEEE Microwave and Guided Wave Letters*, vol. 5, no. 11, pp. 368–370, 1995.

[49] W. Strupinski, L. Dillner, J. Sass, K. Kosiel, J. Stake, M. Ingvarson, and R. Jakiela, “MOVPE strain layers - growth and application,” *Journal of Crystal Growth*, vol. 221, pp. 20–25, 2000.

[50] M. Ingvarson, L. Dillner, W. Strupinski, and J. Stake, “Design of material structures for heterostructure barrier varactors,” in *Presented at the 19th Nordic Semiconductor Meeting*, 2001.

[51] M. Ingvarson, A. Ø. Olsen, B. Alderman, and J. Stake, "Heterostructure barrier varactor frequency multipliers: materials, devices and circuits," in *Proceedings of GHz 2001*, Lund, 2001.

[52] E. Lheurette, X. Mélique, P. Mounaix, F. Mollot, O. Vanbésien, and D. Lippens, "Capacitance engineering for InP-based heterostructure barrier varactor," *IEEE Electron Device Letters*, vol. 19, no. 9, pp. 338–340, 1998.

[53] J. Stake, L. Dillner, and E. Kollberg, "Investigation of an InAs based heterostructure barrier varactor," in *Proceedings of GHz 1995*, 1995, pp. PS33–34.

[54] K. Inoue, J. C. Harmand, and T. Matsuno, "High-quality $In_xGa_{1-x}As$/InAlAs modulation doped heterostructures grown lattice-mismatched on GaAs-substrates," *Journal of Crystal Growth*, vol. 111, no. 1-4, pp. 313–317, 1991.

[55] T. Mishima, K. Higuchi, M. Mori, and M. Kudo, "High g_m $In_{0.5}Al_{0.5}As/In_{0.5}Ga_{0.5}As$ high electron mobility transistors grown lattice-mismatched on GaAs substrates," *Journal of Crystal Growth*, vol. 150, pp. 1230–1235, 1995.

[56] M. Saglam, K. Mutamba, A. Megej, C. Sydlo, and H. L. Hartnagel, "Influence of polarization charges in $Al_{0.4}Ga_{0.6}N$/GaN barrier varactors," *Applied Physics Letters*, vol. 82, no. 2, pp. 227–229, 2003.

[57] J. M. DiDomenico, D. A. Johnson, and R. H. Pantell, "Ferroelectric harmonic generator and the large-signal microwave characteristics of a ferroelectric ceramic," *Journal of Applied Physics*, vol. 33, no. 5, pp. 1697–1706, 1962.

[58] P. Rundqvist, "Perovskite oxides for parallel plate ferroelectric varactors," Chalmers University of Technology, Tech. Rep. 488L, 2004.

[59] R. Williams, *Modern GaAs processing methods, 2nd ed.* Artech House, 1990.

[60] L. Dillner, J. Stake, and E. L. Kollberg, "Heterostructure barrier varactors on copper substrate," *Electronics Letters*, vol. 339 - 341, no. 4, pp. 339–341, 1999.

[61] J. Stake, "Planar heterostructure barrier varactor diodes for millimetre wave applications," Ph.D. dissertation, Chalmers University of Technology, 1999.

[62] J. Stake, L. Dillner, S. H. Jones, C. M. Mann, J. Thornton, J. R. Jones, W. L. Bishop, and E. L. Kollberg, "Effects of self-heating on

planar heterostructure barrier varactor diodes," *IEEE Transactions on Electron Devices*, vol. 45, no. 11, pp. 2298–2303, 1998.

[63] J. Stake, C. Mann, L. Dillner, M. Ingvarson, S. H. Jones, S. Hollung, H. Mohamed, B. Alderman, M. Chamberlain, and E. Kollberg, "Improved diode geometry for planar heterostructure barrier varactors," in *Proceedings of the 10th International Symposium on Space Terahertz Technology*, Charlottesville, 1999, pp. 485–491.

[64] B. Alderman, J. Stake, L. Dillner, D. P. Steenson, M. Ingvarson, E. Kollberg, C. Mann, and J. Chamberlain, "A new pillar geometry for heterostructure barrier varactor diodes," in *Proceedings of the 12th International Symposium on Space Terahertz Technology*, 2001, pp. 330–339.

[65] R. Meola, J. Freyer, and M. Claassen, "Improved frequency tripler with integrated single-barrier varactor," *Electronics Letters*, vol. 36, no. 99, pp. 803–804, 2000.

[66] S. Arscott, P. Mounaix, and D. Lippens, "Transferred InP-based HBVs on glass substrate," *Electronics Letters*, vol. 35, no. 17, pp. 1493 – 1494, 1999.

[67] T. David, S. Arscott, J. M. Munier, T. Akalin, P. Mounaix, G. Beaudin, and D. Lippens, "Monolithic integrated circuits incorporating InP-based heterostructure barrier varactors," *IEEE Microwave and Wireless Component Letters*, vol. 12, no. 8, pp. 281 – 283, 2002.

[68] A. Emadi, J. Vukusic, M. Ingvarson, T. Bryllert, Ø. Olsen, E. Kollberg, and J. Stake, "High power HBV multipliers for F- and G- band applications," in *Proceedings of the Joint 29th IRMMW2004 / 12th THz2004*, 2004, pp. 319–320.

[69] M. Tutt, G. I. Ng, D. Pavlidis, and J. Mansfield, "Reliability issues of InAlAs/InGaAs high-electron mobility transistors," in *Proceedings of the 3rd International Conference on Indium Phosphide and Related Materials*, 1991, pp. 349–352.

[70] R. Kamoua and H. Eisele, "Theoretical and experimental comparison of optimized doping profiles for high-performance InP Gunn devices at 220-500 GHz," in *MTT-S International Microwave Symposium Digest*, 2003, pp. 907–910.

[71] S. M. Sze, *Physics of Semiconductor Devices, 2nd ed.* John Wiley & Sons, 1981.

[72] C. H. Page, "Harmonic generation with ideal rectifiers," *Institute of Radio Engineers - Proceedings*, vol. 46, pp. 1738–1740, 1958.

[73] R. H. Pantell, "General power relationships for positive and negative nonlinear resistive elements," *Institute of Radio Engineers - Proceedings*, vol. 46, no. 12, pp. 1910–1913, 1958.

[74] E. L. Kollberg, J. Stake, and L. Dillner, "Heterostructure barrier varactors at submillimetre waves," *Philosophical Transactions of the Royal Society London A*, vol. 354, no. 1717, pp. 2383–2398, 1996.

[75] S. A. Maas, *Nonlinear Microwave and RF Circuits, 2nd ed.* Artech House, 2003.

[76] S. Hollung, J. Stake, L. Dillner, M. Ingvarson, and E. Kollberg, "A distributed heterostructure barrier varactor frequency tripler," *IEEE Microwave and Guided Wave Letters*, vol. 48, no. 4, pp. 24–26, 2000.

[77] W. H. Chow, D. P. Steenson, T. T. Piotrowski, A. Piotrowska, and K. Golaszewska, "An integrated micromachined waveguide frequency tripler for nonlinear wave propagation," in *Proceedings of the IEEE Antennas and Propagation Society Symposium*, 2004, pp. 1563–1566.

[78] A. Ø. Olsen, J. Stake, M. Ingvarson, D. P. Steenson, and S. Iezekiel, "A new waveguide integrated microstrip heterostructure barrier varactor (hbv) frequency tripler," in *Proceedings of the 9th International Conference on Terahertz Electronics*, Charlottesville, 2001.

[79] S. Hollung, J. Stake, L. Dillner, and E. Kollberg, "A 141 GHz quasi-optical HBV diode frequency tripler," in *Proceedings of the 10th International Symposium on Space Terahertz Technology*, 1999, pp. 492–500.

[80] M. Ingvarson, L. Dillner, S. Hollung, E. Kollberg, C. Mann, and J. Stake, "Computer controlled measurements on millimetre and submillimetre wave varactor multipliers," in *Proceedings of GHz 2000*, 2000, pp. 297–300.

[81] K. Krishnamurthi, E. Boch, and R. G. Harrison, "A Ka-band planar tripler based on a stacked symmetric InP heterostructure-barrier varactor," in *IEEE MTT-S International Microwave Symposium Digest*, 1995, pp. 549–552.

[82] H. X. L. Liu, L. B. Sjogren, C. W. Domier, J. N. C. Luhmann, D. L. Sivco, and A. Y. Cho, "Monolithic quasi-optical frequency tripler array with 5-W output power at 99 GHz," *IEEE Electron Device Letters*, vol. 14, no. 7, pp. 329–331, 1993.

[83] D. Choudhury, M. A. Frerking, and P. D. Batelaan, "A 200 GHz tripler using a single barrier varactor," *IEEE Transactions on Microwave Theory and Techniques*, vol. 41, no. 4, 1993.

[84] X. Mélique, A. Maestrini, E. Lheurette, P. Mounaix, M. Favreau, O. Vanbésien, J. M. Goutoule, G. Beaudin, T. Nähri, and D. Lippens, "12% efficiency and 9.5 dBm output power from InP-based heterostructure barrier varactor triplers at 250 GHz," in *IEEE MTT-S International Microwave Symposium Digest*, 1999.

[85] M. Saglam, B. Schumann, K. Duwe, C. Domoto, A. Megej, M. Rodriguez-Girones, J. Muller, R. Judaschke, and H. Hartnagel, "High-performance 450-GHz GaAs-based heterostructure barrier varactor tripler," *IEEE Electron Device Letters*, vol. 24, no. 3, pp. 138 – 140, 2003.

[86] A. V. Räisänen, T. J. Tolmunen, M. Natzic, M. A. Frerking, E. Brown, H. Grönqvist, and S. M. Nilsen, "A single barrier varactor quintupler at 170 GHz," *IEEE Transactions on Microwave Theory and Techniques*, no. 3, pp. 685–688, 1995.

[87] Q. Xiao, Y. Duan, J. L. Hesler, T. W. Crowe, and R. M. Weikle II, "A 5-mW and 5% efficiency 210 GHz InP-based heterostructure barrier varactor quintupler," *IEEE Microwave and Wireless Component Letters*, vol. 14, no. 4, pp. 159–161, 2004.